Microfluid Nanofluid (2017) 21:147
DOI 10.1007/s10404-017-1985-5

RESEARCH PAPER

Analytical solution of micro-/nanoscale convective liquid flows in tubes and slits

Gulce Kalyoncu[1] · **Murat Barisik**[2]

Received: 26 February 2017 / Accepted: 9 August 2017 / Published online: 18 August 2017

Abstract Analytical solutions examining heat transport in micro-/nanoscale liquid flows were developed. Using the energy equation coupled with fully developed velocity, we solved developing temperature profiles with axial conduction and viscous dissipation terms. A comprehensive literature review provided the published range of velocity slip and temperature jump conditions. While molecular simulations and experiments present constant slip and jump values for a specific liquid/surface couple independent of confinement size, non-dimensional forms of these boundary conditions were found appropriate to calculate non-equilibrium as a function of flow height. Although slip and jump conditions are specific for each liquid/surface couple and hard to obtain, we proposed modeling of the slip and jump as a function of the surface wetting, in order to create a general, easy to measure methodology. We further developed possible correlations to calculate jump using the slip value of the corresponding surface and tested in the results. Fully developed *Nu* showed strong dependence on slip and jump. Heat transfer stopped when slip and jump coefficients became higher than a certain value. Strong variation of *Nu* in the thermal development length was observed for low slip and jump cases, while an almost constant *Nu* in the flow direction was found for high slip and jump coefficients. Variation of temperature profiles was found to dominate the heat transfer through the constant temperature surface while surface and liquid temperatures became equal at heat transfer lengths comparable with confinement sizes for no-dissipation cases. In case of non-negligible heat dissipation, viscous heating dominated the *Nu* value by enhancing the heating while decreasing the heat removal in cooling cases. Implementation of proposed procedure on a micro-channel convection problem from a micro-fluidics application showed the dominant effect of the model defining the slip and jump relationship. Direct use of kinetic gas theory resulted in an increase of *Nu* by an increase in non-equilibrium, while models developed from published liquid slip and jump values produced an opposite behavior.

Keywords Velocity slip length · Velocity slip coefficient · Kapitza length · Temperature jump coefficient · Axial conduction · Viscous dissipation

1 Introduction

The interest in using micro-/nanoscale liquid convection for various applications has been growing rapidly due to the recent popularity of micro-/nano-devices in chemical processes (Yoshida et al. 2011; Su et al. 2014), biomedical/mechanical applications (Koev et al. 2010; Qiu et al. 2014), electronical cooling systems (Iverson et al. 2009; Kuo and Hsu 2013), and the aerospace industry (Manca et al. 2011). However, diversions from continuum assumption make analyzing fluid dynamics in small scales rather difficult, since many of the non-continuum mechanisms are still not completely understood as much as conventional flow systems. Specifically, for liquid flows, characterizing and calculating so-called non-equilibrium effects are very challenging compared to well-known micro-/nano-gas dynamics. Existing literature is very limited and includes misleading characterization attempts, such that a proper consideration of micro-/nano-liquid dynamics coupled with effects originated from

✉ Murat Barisik
muratbarisik@iyte.edu.tr

[1] Energy Engineering MSc. Programme, Izmir Institute of Technology, 35430 Izmir, Turkey

[2] Mechanical Engineering Department, Izmir Institute of Technology, 35430 Izmir, Turkey

low flow speeds, short heating lengths, and large length-to-diameter ratios of micro-/nanoscale applications is vital for future technologies.

At micro-/nano-levels, the interactions between fluid and surface become dominant and create non-equilibrium behaviors in fluid dynamics so that classical continuity-based theories cannot resolve the heat and mass transport. These small-scale effects are observed differently in the case of a liquid flow rather than a gas case. Gas flow at micro-/nanoscales is a well-studied subject due to the convenient calculations provided by Kinetic Theory (KT) and Molecular Dynamics (MD). However, small-scale effects on liquid flows are not that simple to estimate. This deficiency is mostly caused by the complex momentum exchange behaviors of liquid molecular system in which the collision dynamics cannot be calculated using Kinetic Theory of gases due to the high density. Hence, the Kn number cannot be defined for liquids and related theories and solution procedures cannot be applied. There are multiple studies defining Kn and employing KT-based solutions such as Maxwell defined velocity slip and temperature jump models as a function of Kn for liquid flows (Mirramezani and Mirdamadi 2012; Rashidi et al. 2012; Matin et al. 2013; Bardia et al. 2016) as well as for characterization of nano-fluids (liquids containing nanoparticles) (Buongiorno 2006; Hooman et al. 2009; Hooman and Ejlali 2010; Akbarinia et al. 2011; Yang et al. 2015) which are misleading researchers to an incorrect physical interpretations of liquid flows at micro-/nanoscale.

On the other hand, there are no existing theories to generally characterize liquid non-equilibrium behaviors and their length scales. The molecular surface forces and adsorption develop different mechanisms than gas state. Basically, non-equilibriums are observed at the liquid/solid interface momentum and energy exchange coupling, as well as at the near interface liquid dynamics. Velocity slip and temperature jump develop at the interface between surface and liquid while density layering and electric double layer (EDL) are two major complications forming in liquid at near interface. But, the length scales of near interface non-equilibrium regions are very small such that its contribution is negligible for even very small confinements. Hence, over a certain dimensional limit (further discussions are in Sect. 2), defining an updated boundary condition for an overall consideration of the non-equilibrium effects can be performed.

Multiple researchers attempted to solve micro-/nanoscale liquid convective flows with the velocity slip and temperature jump boundary conditions in order to include non-equilibrium effects. Specifically, Enright et al. (2010) and Cowley et al. (2016) showed a decrease in overall heat transfer coefficient due to the increase in temperature jump, for superhydrophobic channels. Khare et al. indicated that velocity slip increases interfacial thermal resistance. However, there is a knowledge gap about possible velocity slip and temperature jump range and their theoretical considerations in a non-dimensional form (Khare et al. 2006).

There are additional mechanisms which become dominant at microscales. First, heat transfer occurring through the thermal development length becomes a major mechanism in many microscale heat exchangers. Second, small Reynold numbers ($Re = (V \times D_H)/\nu$, where V is flow speed and ν is kinematic viscosity) of the micro-flows result in small Peclet numbers ($Pe = Re \times Pr$ where Pr is the Prandtl number); and hence, the axial conduction cannot be neglected as the convection term no longer dominates the conduction term in the axial direction. This effect especially dominates the thermally developing region of heat transfer. Third, the small confinements create large length-to-diameter ratios which develop viscous heating, and the effect of viscous dissipation becomes significant as the wall-to-fluid temperature difference becomes small in micro-convection (non-negligible Brinkman number). The viscous dissipation prolongs the thermal development through the flow direction and dominates the fully developed heat transfer.

The effects of thermal development region, axial conduction, and viscous dissipation were attempted to be combined with liquid velocity slip and temperature jump in the literature. For example, axial conduction was studied by Cole and Cetin, and they concluded that the effect of axial conduction becomes dominant for small Pe numbers, especially at microscales (Cole and Cetin 2011). Similarly, in the study conducted by Cowley et al. for water flow through superhydrophobic walls with slip and jump, it was found that overall Nu number decreases as the Pe number decreases (Cowley et al. 2014). Koo and Kleinstreuer (2003), and Morini and Spiga (2007) studied the viscous effects in the micro-channels and concluded that dissipation dominates the heat transfer characteristics. Shojaeian and Kosar also studied the viscous dissipation with the velocity slip where they observed the decrease in dissipation effects for systems having high slippage (Shojaeian and Kosar 2014). However, there is not any complete coupling of all effects for micro-/nanoscale liquid convection. Especially, heat transfer in micro-/nano-slits and tubes at low Pe with non-negligible viscous heating through thermal development length, which occasionally extends up to ten times the flow height, needs to be calculated to support current applications. Recently, we overcame the mathematical challenge and solved the energy equation including axial conduction and viscous dissipation terms (Barisik et al. 2015; Kalyoncu and Barisik 2016).

The solution for convective heat transport in micro-/nanoscale confinements will provide valuable insight for the current thermal management attempts. Parallel to the increasing needs for temperature control systems in numerous applications, engineers have been focused on smart and green heat management solutions. Specifically, heat storage using phase change materials (PCM) has become one of the main attractions for efficient energy removal, conversion, conservation, and reuse (Zalba et al. 2003; Viskanta 1983, 1985). For example, the new NASA project, Phase Change Heat Exchanger (PCM-HX), is currently testing such an idea to maintain a safe temperature in a spacecraft (NASA 2017). Simply, the wax material inside PCM-HX can store thermal energy in form of latent heat that PCM-HX converts the excess heat removed and conserves it to use for future needs. The solidification and melting process during the storing and releasing heat occur at a constant temperature such that PCM develops a constant temperature on its container. Hence, with the trend for decrease in flow scales, heat transfer between heat exchanger liquid and the PCM container surface in a PCM-HX system requires micro-/nanoscale liquid convection calculations over a constant temperature surface.

The objective of this study is to expand on the earlier developed analytical approach to devise a solution for hydrodynamically developed, thermally developing liquid flow in micro-tubes and slits by coupling velocity slip, temperature jump, viscous dissipation, and axial conduction for a constant surface temperature. For such a case, velocity slip and temperature jump measurements from existing literature will be summarized and results will be normalized by corresponding channel heights to develop a possible range of slip and jump conditions for non-dimensional analytical solution. We will further describe the boundary condition in terms of contact angles. We will present the heat transfer characteristics of liquid flow in the presence of different velocity slip and temperature jump effects under different viscous heating and axial conduction in the thermally developing convection.

2 Micro-/nanoscale non-equilibrium effects on fluid transport

In general, non-equilibrium fluid dynamics developing due to the disturbance from the presence of a surface occurs near the boundaries. The extension of this behavior into a fluid domain should be determined as a first step to characterize micro-/nanoscale effects. In gas flows, the Knudsen number ($Kn = \lambda/D_H$) calculated as the ratio of gas mean free path (λ) to the characteristic height of confinement (D_H is the hydraulic diameter) provides an understanding of non-equilibrium gas dynamics, while the B parameter ($B = L_f/D_H$) calculated as the ratio of surface molecular force penetration depth to characteristic height of confinement considers the effect of surface forces which are dominant at nanoscales (Barisik et al. 2010; Barisik and Beskok 2011a, 2012a, 2014a, 2015, 2016). However, in comparison with well-understood micro-/nanogas flow dynamics, non-equilibrium behavior in liquid flows is not easy to calculate. Liquid systems undergo multibody collisions and interact through molecular forces dominantly such that a "mean free path" like definition does not exist. Instead, one may calculate an average spacing between liquid molecules to compare some possible interaction length scales to the size of confinement. Since the average molecular spacing of water at standard conditions is as small as a molecular diameter (0.3 nm) (Milo and Phillips 2015), non-equilibrium liquid dynamics are not expected to develop in the regions sufficiently away from the surface. Instead, non-continuum behaviors are expected to be confined mostly in interface regions. For such a case, near surface liquid behavior is required to be resolved in order to calculate its extent. Experimental measurements [atomic force microscopy (AFM)] and molecular dynamics (MD) simulations provide molecular level resolution of near surface liquid structures and non-continuum behaviors (Maali and Bhushan 2012). First, a solid-like liquid ordering named as "density layering" is observed on solids extending a couple of molecular diameters (~1 to 2 nm) approximately from a non-charged surface (Barisik and Beskok 2011b). Second, liquid systems contain dissolved ions which interact with the charged surface and form the electrical double layer (EDL) as thick as 300 nm depending on ionic concentration (Dutta and Beskok 2001; Barisik and Beskok 2014b; Barisik et al. 2014; Atalay et al. 2014); but, electrokinetic forces are effective if the ionic layer is thin (<1–2 nm). Hence, fluid properties and dynamics diverge from the continuum description inside these near surface formations. The dimensional limit of a possible continuum-based description for liquid micro-/nano-flows can be determined by comparing the length of this non-equilibrium region to the confinement size. For example, for a high ionic concentration and low surface charge and wetting case, near surface non-equilibrium (EDL and layering) covers less than a couple nanometers, and hence, liquid flow and thermal conduction can be calculated by NS and Fourier Law using velocity slip and temperature jump boundary conditions for channels as small as 50 nm (Shi et al. 2012). This validates that near interface non-homogeneous density and ionic distributions are mostly dominant in a limited part of the liquid flow domain and the solution of conservation equations with an updated momentum and energy boundary conditions considering non-equilibrium effects appears to be a good tool to solve micro-/nano-liquid flows. This can be considered as a great advantage of liquid systems. However, no theories exist to calculate

required velocity or temperature boundary conditions as a function of near surface non-equilibrium liquid dynamics; instead, they are mostly determined by experiments and MD. Furthermore, there is no conclusion about the dependence of these boundary conditions to liquid/solid interaction properties and flow conditions. The following chapters present a wide literature survey on velocity slip (Sect. 2.1), temperature jump (Sect. 2.2) at solid liquid interfaces, and their dependence on the wetting angle (Sect. 2.3) of corresponding surfaces.

2.1 Slip velocity and slip length at the boundary

Liquid velocity at a boundary presents various conditions among slip, no-slip, and even stick of multiple molecular layers (Koumoutsakos 2003). While the velocity stick is mostly effective for channels smaller than ten molecular diameter size (Xu and Li 2007), it is considered as no-slip for the rest of the scales. No-slip condition is common for superhydrophilic and rough surfaces. But, many of the recent technologies employ atomisticly smooth boundaries where strong slip develops. The idea about the velocity slip was first proposed by Navier (1823). According to the Navier's well-known boundary conditions, the velocity at the surface, v_{slip}, is proportional to shear stress at the wall (Gad-el-Hak 1999).

$$v_{\text{slip}} = L_s \left.\frac{\mathrm{d}v}{\mathrm{d}y}\right|_{@\text{wall}} \tag{1}$$

where $\left.\frac{\mathrm{d}v}{\mathrm{d}y}\right|_{@\text{wall}}$ is the velocity gradient at the wall and L_s is the slip length. Slip length measures the velocity slip as a fictitious distance at which the velocity extrapolates to the value of zero. Slip length is expected to depend on properties of solid and liquid couples as well as on the flow dynamics. In the literature, research has been focused on the effects of interfacial properties (Jabbarzadeh et al. 1999; Barrat and Bocquet 1999; Cottin-Bizonne et al. 2002; Koumoutsakos et al. 2003; Cho et al. 2004; Schmatko et al. 2005; Voronov et al. 2006, 2007; Huang and Breuer 2007; Huang et al. 2008; Sendner et al. 2009; Sun et al. 2012; Sofos et al. 2013; Zhang and Chen 2014; Yen 2015; Yen and Soong 2016; Ramos-Alvarado et al. 2016), shear rate (Jabbarzadeh et al. 1999; Craig et al. 2001; Choi et al. 2003; Joseph and Tabeling 2005; Li et al. 2014), and channel height (Cheng and Giordano 2002; Lichter et al. 2007; Xu and Li 2007; Lee et al. 2012) on slip length. The extensive literature survey shows that studies about the dependence of slip length on the surface and flow properties are widespread, and there is a consensus about the direct relationship between slip length, liquid/solid interaction energies, and shear rate.

Conversely, L_s and channel height dependency are not as clear as conclusions about the dependency on most of the other parameters. For example, some researchers claim that L_s is independent of the channel height. Cheng and Giordiano developed this conclusion for Poiseuille's flow experiments by Cheng and Giordiano at scales between 2.7 and 40 μm (Cheng and Giordano 2002). Similarly, Bizonne et al. concluded that there is no relation between slip and the scale of the flow domain in the range of 1 to several hundreds of nanometers (Cottin-Bizonne et al. 2005). Recently, Ghorbanian and Beskok presented the variation of slip length by surface properties while it remained constant for a certain liquid/solid couple at any size of confinement (Ghorbanian and Beskok 2016). For such a case, the ratio of the constant slip length of a given liquid/surface couple with the corresponding flow height can provide a prediction of slip effects onto liquid flow inside different size conduits. Also, known as slip coefficient (β), the slip length non-dimensionalized with channel height can be utilized to calculate micro-/nanoscale effects into the NS solution as a function of confinement's size. While the slip length remains constant, an increase in channel height decreases the slip effects and flow behavior approaches the no-slip continuum solution. Thus, the contribution of velocity slip to liquid transport can be characterized by slip coefficient calculated at the conduit size.

On the other hand, there are also studies presenting variations of slip length based on the confinement size (Lichter et al. 2007). Multiple studies on water flow in carbon nanotube (CNT) showed that an increase in CNT diameter decreases the slip length gradually (Thomas et al. 2010; Suk and Aluru 2013; Yasuoka et al. 2015). In that case, the NS solution became complicated since the normalized NS solution based on dynamic similarity was impossible. Instead, any slip coefficient required for the NS solution of a certain confinement height should be calculated based on the slip length of the corresponding size. In this case, models developed for the variation of slip length with the channel height (Yang and Zheng 2010) can be useful for NS-based theoretical solutions. For example, one can utilize the models developed by Suk and Aluru as $L_s = 0.205 + 0.1517/R$ (nm) (2013), or by Thomas et al. as $L_s = 30 + 44/R^3$ (nm) (2010) where R is the nanotube radius. While presenting an exponential increase in slip length with an increase in channel height at very small scales, these studies also represent that the slip length converges to a constant value and becomes independent to channel height for confinement sizes bigger than ~10 nm. Hence, the idea of using slip coefficient to incorporate slip effects as a function of conduit size can be valid for channels as small as 10 nm.

Table 1 Summary of the slip lengths and the slip coefficient (β) based on corresponding conduit sizes from the literature

References	Channel height (nm)	Tube diameter (nm)	Slip length (nm)	β	Solid/liquid material
Tretheway and Meinhart (2002)	3×10^4		1000	0.033	OTS/DI water
Choi et al. (2003)	10^3–2×10^3		30	0.03–0.015	OTS/DI water
Koumoutsakos et al. (2003)		4.72–4.50	63–31	13.34–6.88	Graphite/water
Ou et al. (2004)	127×10^3		10^3–21×10^3	0.008–0.16	Silicon/water
Kassinos et al. (2004)		5.424	18	3.31	CNT/water
		2.712	10	3.68	
		4.068	12	3.44	
Majumder et al. (2005)		7	39×10^3	5571	MWCNT/water
			68×10^3	9714	
Chun and Lee (2005)	10^6		6×10^3–8×10^3	6×10^{-3}–8×10^{-3}	PDMS/water
Joseph and Tabeling (2005)	10^5		<100	$<10^{-3}$	PDMS/DI water
Holt et al. (2006)		15	5.1	0.34	Polycarbonate/water
		1.6	140–1400	87.5–875	DWNT/water
Cao et al. (2006)	10.2		7.9	0.77	Platinum/argon
Choi and Kim (2006)	3×10^3		100–200	0.033–0.066	Silicon/water
Lichter et al. (2007)	0.14		0.44	3.14	FCC representative Surface/*n*-decane
	1.4		1.96	1.4	
Huang and Breuer (2007)	5×10^4		100	2×10^{-3}	PDMS/DI water
Byun et al. (2008)	2×10^5		2×10^3	0.01	PDMS/water
Thomas and McGaughey (2008)		1.66–4.99	30	18.07–6.01	Graphene/water
Martini et al. (2008)	3		2–22.0	0.17–1.83	FCC representative Surface/*n*-decane
Whitby et al. (2008)		44	26–35	0.6–0.8	CNT/water
Thomas et al. (2010)		1.5–5	115–30	6–76.6	Graphene/water
Falk et al. (2010)		1	500	500	CNT/water
		7	120	17.14	
Qin et al. (2011)		0.81	53	65.43	CNT/water
		1.59	8	5.03	
Majumder et al. (2011)		34×10^3 –126×10^3	53.3	1.56×10^{-3} –4.23×10^{-4}	CNT/water
Groombridge et al. (2011)		3	1.325–1.231	0.44–0.41	CNT/water
		4	1.069–1.151	0.27–0.29	
		6	1.018–1.097	0.17–0.18	
		9	1.087–1.072	0.12	
		12	1.207–1.222	0.1–0.102	
Roy et al. (2013)	30–2×10^5		0–10^3	0.005–33.3	FCC representative surface/water
Li et al. (2014)	100		3.66	0.01	Silicon/DI water
Rogers and Wirth (2012)	15–800		63	4.2–0.078	Silica colloidal crystals/water

OTS octadecyltrichlorosilane, *DI* deionized, *MWCNT* multiwalled CNT, *DWNT* double-walled CNT, *PDMS* polydimethylsiloxane

In summary, numerous reported slip lengths for different liquid/solid couples at various conditions exist. Despite the existing attempts to develop a theoretical slip model for liquid flows, there is no generally accepted conclusion. At this point, our preliminary target is to determine a physical range of slip length and slip coefficient from existing systems studied in the literature. A diverse amount of studies on direct or indirect measurements of slip length are summarized in Table 1 which presents the measured slip length values, corresponding characteristic lengths of conduits, and resulted slip coefficients. Slip lengths as high as 400 μm (Lee and Kim 2009) can be observed from the tabulated results. Assuming that the slip length is only defined by surface/liquid coupling and remains constant,

the slip coefficient value could be negligible in a 10-m tube while a 10-nm tube will create a slip coefficient on the order of 10^4. In addition to this perspective, we also attempted to determine the highest value for a slip coefficient directly from published values. Similar slip coefficient ranges as high as 10^4 were observed (Majumder et al. 2005).

2.2 Temperature jump and Kapitza length at the boundary

The temperature jump develops due to a mismatch at phonon dispersions between two dissimilar materials forming the interface. The jump can be specified by the Kapitza length (L_K) measured by extrapolating the temperature profile from liquid into the solid, where the wall temperature is reached as,

$$\Delta T_i = L_k \frac{\partial T}{\partial y}\bigg|_{@wall} \tag{2}$$

In Eq. (2), ΔT_i is the difference between fluid and wall temperatures at the interface and $\partial T/\partial y$ is the thermal gradient on the liquid side. A literature survey shows that the interface thermal resistance is mostly effective at nanoscales liquid flows. Since direct experimental measurements at such small scales are very challenging and results are imprecise due to fluctuations, Kapitza length measurements have generally been taken using molecular dynamic simulations. Researchers have focused on the relationship between temperature jump and parameters of liquid and surface. In particular, Kapitza resistance at solid/liquid interfaces is found to depend significantly on relative molecular thermal oscillation frequencies (Kim et al. 2008), solid/liquid interaction strength (Kim et al. 2008; Kou and Bai 2011), liquid pressure (Pham et al. 2014), wall temperature (Barisik and Beskok 2012b, 2014b), and surface topology (Ge et al. 2006; Kim et al. 2008, 2010; Shi et al. 2012). However, a theoretical model with complete understanding is still missing. While depending on the solid and liquid properties strongly, Kapitza length was found to be a constant independent of the channel for channels as small as 10 nm height (Shi et al. 2012). Hence, based on corresponding conduit size, a non-dimensional form of Kapitza length specified as the jump coefficient (α) can be utilized as a NS boundary condition to calculate micro-/nanoscale temperature jump effects as a function of system size. For such a case, existing Kapitza length measurements from the literature are tabulated in Table 2 with corresponding confinement sizes and jump coefficients.

Furthermore, both the velocity slip and temperature jump conditions are developed using very similar mechanisms from liquid/solid interfacial coupling that is expected to have a close correlation between slip and jump behaviors. Unfortunately, there have been very few attempts for modeling temperature jump in a relation with velocity slip of corresponding surface in the literature.

The existing practice of assuming a negligible temperature jump while considering substantial velocity slip in the literature is misleading since L_s and L_k develop

Table 2 Summary of the Kapitza lengths and the jump coefficient (α) based on corresponding channel heights from the literature

Study	Kapitza length (nm)	Channel height (nm)	α	Solid/liquid material
Kim et al. (2008)	13	3.24	4.01	Representative FCC surface/argon
Barisik and Beskok (2012b)	0.53–1.11	7	0.075–0.158	Silver/argon
	0.3–0.94		0.042–0.134	
Shi et al. (2012)	0.97–1.23	7	0.14–0.17	Silver/argon
	3.1–3.5	3.57	0.86–0.94	Graphite/argon
Pham et al. (2013)	6.5–6.9	6.9	0.94	Gold/water
	7.5–6	6.5	1.07–0.92	Silicon/water
Pham et al. (2014)	1.5–2.8	6.518	0.23–0.429	Silicon/argon
	6		0.92	Silicon/water
Barisik and Beskok (2014b)	2.98–14.76	6.4	0.46–2.31	Silicon/water
	2.69–16.26		0.42–2.54	
Vo and Kim (2015)	8.5	8	1.06	Silicon/water
	14.2	7.8	1.82	Copper/water
	7	7.6	0.92	Gold/water
	4	7.2	0.55	Platinum/water
	2.8	7.5	0.37	Silver/water
Pham et al. (2016)	9–46	7	0.77–6.57	Graphene-coated Cu (111)/water

Table 3 Measured slip and Kapitza length values, the linear relations obtained via data extraction, and the proposed relations as a part of boundary conditions

Study	L_s (nm)	L_k (nm)	$L_k = \kappa \times L_s$	κ
Kou and Bai (2011)	0.4–2.2	1.84–11.35	$L_k = 3.03\ L_s$	3.03
Sun et al. (2013b)	5.29–8.52	0.49–17.14	$L_k = 4.87\ L_s$	4.87
Sun et al. (2013a, b)	1.64–4.55	1.89–22.24	$L_k = 7.13\ L_s$	7.13
Roy et al. (2013)	–		$L_k = 0.13\ L_s$	0.14
Thekkethala and Sathian (2015)	17.7–28.78	0.06–6.90	$L_k = 0.61\ L_s$	0.61

simultaneously as a function of surface properties. Just recently, researchers attempted to reveal a possible analogy between L_k and L_s (Pham et al. 2013, 2014, 2016; Roy et al. 2013; Thekkethala and Sathian 2015; Vo and Kim 2015). Table 3 summarizes the measured slip length ranges together with the Kapitza length ranges for the same surface and flow conditions. In addition to simultaneous measurements of slip and jump, Sun et al. attempted to develop a model for the L_s and L_k relationship. Their MD results at various flow and surface conditions showed that L_k gets almost negligible values at velocity conditions of locking to small slip after which L_k showed an exponential increase with the increase of L_s. Although useful, their proposed model is too complex to implement in a continuum-based solution. On the other hand, a simpler approximation for the L_s and L_k relation has been practiced for gas flows based on the Prandtl number (Pr). Pr calculates the ratio of momentum diffusivity to thermal diffusivity which also defines shear stress and heat flux at the interface. Hence, the Pr value of corresponding gas provides the ratio of slip length to Kapitza length as $L_k = L_s/Pr$ (Roy et al. 2013). A similar understanding between L_s and L_k is expected to also be observed for liquid flows. However, the linear relationship may develop at different proportionalities at liquid flows since the momentum and heat exchange with surface is more complex than gas flows. For such a case, we applied a linear curve fitting on the L_s versus L_k data given in Table 3 and calculated κ parameters for $L_k = \kappa \times L_s$ relationship. The constant κ gets values between 0.13 and 7.13 while $\kappa = 0.13$ was calculated by directly assuming $L_k \approx Pr \times L_s$ ($Pr = 7.7$ for water at standard conditions). As a result, the non-dimensional solution of energy equation can employ $\alpha = \kappa \times \beta$ as a thermal boundary condition.

2.3 Non-equilibrium surface conditions in terms of wettability

Overall, the micro-/nanoscale non-equilibrium liquid dynamics can be taken into account using velocity slip and temperature jump boundary conditions in NS solution for confinement bigger than certain sizes (~50 nm). However, slip and jump values cannot simply be calculated by any theory; instead, these conditions should be measured by either experiments or molecular simulations specifically for corresponding liquid/solid couples, but this is very challenging and even unfeasible. On the other hand, as the momentum and thermal exchange coupling between liquid and solid is a direct function of interfacial energy, slip and jump conditions can be expressed by surface wetting phenomena and may be simply predicted by contact angle (θ) measurements.

The angle at a liquid–vapor–solid interface is known as the contact angle and can be utilized to qualitatively measure surface wetting. When a drop of liquid is on a solid surface, it may remain as a spherical drop or spread to cover the solid surface. Specifically, wetting occurs when the contact angle is less than 90°, while the liquid does not wet the surface for contact angle values greater than 90°. For such a case, water/solid interactions are classified as hydrophilic if the contact angle is less than 90°, hydrophobic if the contact angle is greater than 90° and superhydrophobic if the contact angle is greater than 150° (Barisik and Beskok 2013; Yeh et al. 2009). Frequently, the relationship between the contact angle, liquid surface tension, liquid/solid interfacial energy, and solid free surface energy is defined by Young's equation. However, other surface properties exist in addition to the contact angle and need to be considered to determine the interaction of liquid with solid surface and wetting behavior. For instance, the surface morphology, also called roughness, is one of the major properties to determine wetting. Wetting of a rough surface can be homogeneous if the liquid fills in the surface roughness or can be heterogeneous if the liquid stays on top of the surface grooves, which are filled with air. For this reason, measured contact angles cannot be correlated with interface tensions using Young's equation; instead, Wenzel's model should be employed for homogenous wetting, while the Cassie–Baxter model can be applicable for heterogeneous wetting of non-flat or composite/textured surfaces.

Multiple researchers investigated the effect of wettability on temperature jump and velocity slip conditions. For homogeneous surfaces at Wenzel wetting state, slip and jump develops directly between solid and liquid. On the other hand, at the Cassie–Baxter wetting, slip and jump are not only the result of liquid–solid momentum coupling, but also due to the interactions between liquid and gas filling the micro-/nano-cavities of heterogeneous surface. For example, the air in cavities may develop almost no shear on liquid flow compared to solid contact with a no-slip condition. For

liquid flowing over a such heterogeneous surface composed of solid and gas, a combined behavior should be calculated for an effective slip condition of the surface. Similar considerations can be done for the temperature jump as well. For the apparent slip and jump conditions developing on heterogeneous surfaces, additional parameters need to be considered in order to properly incorporate the effect of slip associated from the liquid–gas interfaces as a function of solid–gas fraction, in addition to the contact angle, such as: geometrical parameters of air bubble in cavity (Davis and Lauga 2009; Teo and Khoo 2010) and of surface structures (Cheng et al. 2009; Ng and Wang 2010; Woolford et al. 2009).

In a general description, the hydrophilic surfaces were found to develop no-slip and no-jump boundary conditions while the hydrophobicity prevails the slip and jump behavior (Cho et al. 2004; Majumder et al. 2005; Joseph and Tabeling 2005; Lauga et al. 2007; Neto et al. 2005; Cao et al. 2006; Joseph et al. 2006; Voronov et al. 2007; Huang et al. 2008; Kou and Bai 2011; Maali and Bhushan 2012; Roy et al. 2013; Maynes et al. 2013; Enright et al. 2010). However, correlating slip and jump to wetting is not an easy task. For such a case, Huang et al.'s study is one of the first attempts to model slip and jump conditions in terms of wetting as a function of contact angle (Huang et al. 2008). Their correlation was based on the relationship between slip length and the solid–liquid friction coefficient which was estimated by the force autocorrelation function of the Green–Kubo formulation for the total lateral force acting on the surface. Hence, the fluid–solid interaction was associated with the mean squared interaction force related to the square of fluid/solid interaction energy parameter. Similarly, the Laplace estimate of the interfacial tensions is related to the liquid/solid interaction energy in that combining these in Young's equation portrays the relationship between slip length and contact angle (θ_c) as,

$$L_s \approx \left(1 + \cos\theta_c\right)^{-2} \tag{3}$$

Huang et al. performed an extended MD study to measure both the contact angle and slip velocity of surfaces at various interaction strength and conditions. While the results showed very similar behavior with Eq. (3), Sendner et al. carried this discussion further by critiquing the limits of $1 + \cos\theta$ term and proposing Eq. (4) (Sendner et al. 2009).

$$L_s \approx \left(180^\circ - \theta_c\right)^{-2} \tag{4}$$

Equations (3) and (4) were tested for various liquid solid cases by multiple researchers. Yen and Soong studied the relationship between slip length and contact angle for Si (100) and graphite that their results suggested that Huang's findings were only valid for the Cassie-like state (Yen and Soong 2016). The interactions of water with Si (100) and Si (111) also studied by Alvarado et al. where results showed a slightly better match with Eq. (4) than (3) while the slip lengths were strongly dependent on the solid surface molecular density and resulted depletion length (Ramos-Alvarado et al. 2016). Sokhan et al. and Koumoutsakos also identified the dominant effect of solid density on slip length (Sokhan et al. 2001; Koumoutsakos 2003). Voronov et al. studied the effect of molecular size on the slip length and wettability that slip length was found to increase and contact angle to decrease as the molecular diameter for hydrophobic surfaces increased (Voronov et al. 2006, 2007). Effects of liquid polarity were studied by Cho et al., and Eq. (3) was found valid for non-polar liquids while wettability was not found to play an important role on the slip length variation of polar liquids; instead, dipole moments were dominant on slip behavior (Cho et al. 2004). We tabulated the range of wetting angle and corresponding slip measurements from the literature. Table 4 summarizes the published contact angle and slip length ranges measured on different solid/liquid couples, while Fig. 1 presents available data points. We applied proposed relationships given in Eqs. (3) and (4) to all data from very different sources and cases. Even though both models cannot calculate the results of a specific case, the overall behavior between slip length and contact angle can be predicted fairly accurately by these models. Based on the existing data, Eq. (3) shows a better fit in hydrophilic range ($\theta \leq 90$) and Eq. (4) explains behavior in hydrophobic region ($\theta \geq 90$) better.

While studies on slip length versus wetting are extensive, the relationship between contact angle and temperature jump has only been narrowly investigated. Pham et al. measured Kapitza lengths on graphene-coated copper surfaces at different wettings and presented exponential variation on temperature jump by the increase in interaction energy which is a linear function of contact angle. However, the literature is very limited on Kapitza versus contact angle values. For such a case, a relationship between slip length and Kapitza length as introduced earlier in Sect. 2.2 can be employed in order to calculate temperature jump from contact angle values.

3 Analysis

The schematic view of the micro-/nano-channel and tube for the hydrodynamically fully developed and thermally developing liquid flow case is shown in Fig. 2. During the analysis of the problem, incompressible and constant property liquid assumptions were completed. In Fig. 2, the coordinate system is located at the center of two specified geometries. The fully developed velocity profile reaches the heating region where convection starts to develop.

Table 4 Summary of slip length measurements with corresponding contact angle values

Study	Label	Contact angle (°)	Slip length (nm)	Solid/liquid material
Sendner et al. (2009)	S1	48–155	0.49–23.82	Diamond/water
	S2	81.26–143.91	0.82–9.95	Different roughness levels of carbon/water
	S3	77.68–139.42	0.56–7.35	
	S4	58.05–138.45	0.28–6.6	
	S5	91.73–140.88	0.24–4.80	
Yen (2015)	Y1	89.9–150.28	0.52–8.75	Si (100)/water
	Y2	90.76–150	0.25–3.14	
	Y3	91.5–116.94	0.37–0.43	Graphite/water
	Y4	91.73–116.84	1.44–1.19	
Ramos-Alvarado et al. (2016)	A1	152–61.65	4.03–0.08	Si (111)/water
	A2	147.37–60	1.26–0.022	Si (100)/water
Yen and Soong (2016)	YS1	84.108–98.73	0.36–0.14	Si (100)/water
	YS2	113.49–96.30	2.25–0.75	Graphite/water
	YS3	114.36–107.54	2.44–1.12	
	YS4	101.04–113.83	2.85–1.98	

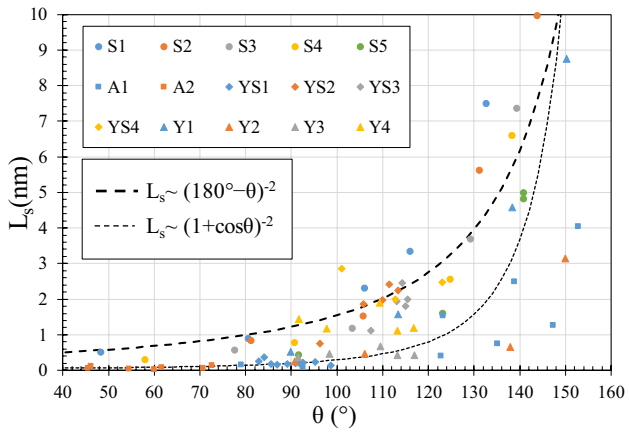

Fig. 1 Slip length values measured at different wetting conditions. Data points were adopted from the literature presented in Table 4. Two models (Eqs. 3, 4) were applied on data

The continuity and Navier–Stokes equations for both Cartesian and cylindrical coordinate systems are given in Eqs. (5), (6a), and (6b). We used the parameter n for a general description, where n equals 0 for the Cartesian geometry and n equals 1 for circular systems.

$$\frac{\partial u}{\partial x}+\frac{\partial v}{\partial y}=0 \tag{5}$$

$$u\frac{\partial u}{\partial x}+v\frac{\partial u}{\partial y}=-\frac{1}{\rho}\frac{\partial p}{\partial x}+\nu\left(\frac{\partial^2 u}{\partial x^2}+\frac{1}{y^n}\frac{\partial}{\partial y}\left(y^n\frac{\partial u}{\partial y}\right)\right) \tag{6a}$$

$$u\frac{\partial v}{\partial x}+v\frac{\partial v}{\partial y}=-\frac{1}{\rho}\frac{\partial p}{\partial y}+\nu\left(\frac{\partial^2 v}{\partial x^2}+\frac{\partial}{\partial y}\left(\frac{1}{y^n}\frac{\partial}{\partial y}(y^n v)\right)\right) \tag{6b}$$

The above given Eqs. (5), (6a), and (6b) were solved using the slip length (Eq. 1) and Kapitza length (Eq. 2) boundary conditions. A general analytical solution and non-dimensional parameter sets were built for both Cartesian and cylindrical coordinate systems by using the parameter n. Similarly, $n=0$ presents solution of Cartesian geometry, and $n=1$ provides the solution for circular geometry. Hydraulic diameter definition (D_h) was employed where $D_h=4H$ for $n=0$, and $D_h=2R$ for $n=1$. The non-dimensional parameters are listed below in Eq. (7).

$$\xi=\frac{3^{n-1}x}{D_h PeB^3 2^{4n-5}} \quad \eta=\frac{y2^{2-n}}{D_h B} \quad \theta=\frac{T-T_W}{T_i-T_w} \quad Pe=RePr$$
$$u^*=\frac{u}{u_{mean}} \quad \widetilde{Pe}=\frac{2^{3n-3}PeB^2}{3^{n-1}} \quad Br=\frac{\mu u_m^2}{k(T_i-T_w)} \quad \beta=\frac{L_s}{D_h}$$
$$A=\frac{1+(2^{3-n}\beta)}{B^2} \quad B=1+\left(12\beta\frac{2^n}{3^n}\right) \tag{7}$$

Solving momentum equations using the boundary conditions Eqs. (8a) and (8b), the non-dimensional velocity (u^*) can be calculated as Eq. (9).

$$y=0\longrightarrow\frac{\partial u}{\partial y}=0 \tag{8a}$$

$$y=2^{n-2}D_h\longrightarrow u=u_s=-L_s\frac{\partial u}{\partial y} \tag{8b}$$

$$u^*=\frac{3^{1-n}2^{2n-1}\left[1+\left(2^{3-n}\beta\right)-\left(y^2 2^{2-n}/D_h\right)^2\right]}{1+\left(3^{1-n}2^{2+n}\beta\right)} \tag{9}$$

The non-dimensionalized form of energy equation containing the axial conduction and viscous dissipation terms with the modified boundary condition for the micro-/nano-liquid flows can be written as follows:

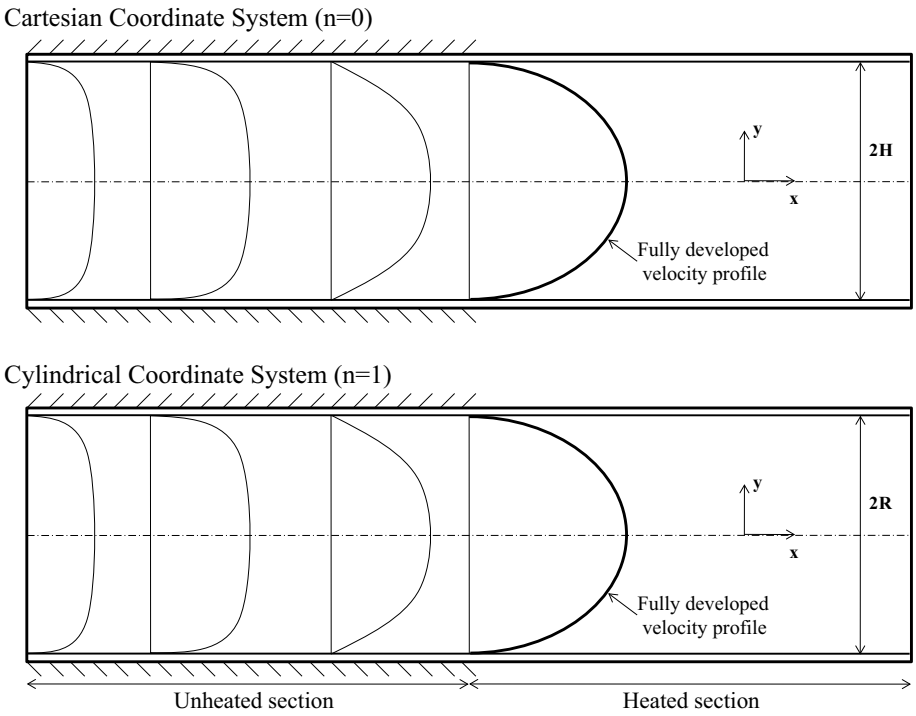

Fig. 2 Studied geometry for the Cartesian and cylindrical coordinates

$$\left(A-\eta^2\right)\frac{\partial\theta}{\partial\xi}=\frac{1}{\eta^n}\frac{\partial}{\partial\eta}\left(\eta^n\frac{\partial\theta}{\partial\eta}\right)+\frac{\partial^2\theta}{\partial\xi^2}\frac{1}{\widetilde{Pe}^2}+Br\left(\frac{\partial u^*}{\partial\eta}\right)^2 \tag{10}$$

$$\eta=0\longrightarrow\frac{\partial\theta}{\partial\eta}=0 \tag{11a}$$

$$\eta={}^1\!/_B\longrightarrow\theta=-\frac{\alpha}{2^{n-2}B}\left(\frac{\partial\theta}{\partial\eta}\right)_{\eta=1/B} \tag{11b}$$

$$\xi=0\longrightarrow\theta=1 \tag{11c}$$

where

$$\alpha=\frac{L_{\mathrm{K}}}{D_{\mathrm{h}}} \tag{12}$$

After the derivation of energy equation using Eqs. (10)–(12), the superposition is applied to the non-dimensional temperature $\theta(\xi,\eta)$,

$$\theta(\xi,\eta)=\theta_1(\xi,\eta)+\theta_\infty(\eta) \tag{13}$$

In Eq. (13), $\theta_\infty(\eta)$ stands for the fully developed thermal profile, while $\theta_1(\xi,\eta)$ is the solution of the homogeneous equation. By substituting Eq. (13) into (10), the fully developed temperature profile for the case of $x\rightarrow\infty$ is written as,

$$\theta_\infty=\frac{Br}{B^2}3^{1-n}2^{1-n}\left[1+\left(2^{n+2}3^{1-n}\right)-\eta^4B^4\right] \tag{14}$$

While the homogenous part of the solution yields to following boundary value problem as,

$$\Theta_1(\xi,\eta)=\sum_{n=1}^{\infty}A_nY_n(\eta)\exp\left(-\lambda_n^2\xi\right) \tag{15}$$

where $Y_n(\eta)$ represents the eigenfunctions, λ_n represents the eigenvalues, and A_n represents the corresponding coefficients (Arfken and Weber 2005). Solution of resulted nonlinear problem requires eigenfunctions as,

$$Y(\eta)=1F1(a,c;z)\exp\left(-\lambda\frac{\eta^2}{2}\right) \tag{16}$$

where $1F1(a,c;z)$ is the Kummer's hypergeometric function while the related coefficients are listed in Table 5.

As the eigenvalues occur nonlinearly, eigenfunctions are not mutually orthogonal compared to the standard Sturm–Liouville problem. In order to calculate the coefficients A_n, Gram–Schmidt orthogonal procedure was used (Dutta et al. 2006). The final form of the temperature distribution $\theta(\xi,\eta)$ was obtained as follows:

$$\theta(\xi,\eta)=A_n1F_1\left(a,c;\lambda_n\eta^2\right)\exp\left(-\lambda_n\frac{\eta^2}{2}\right)\exp\left(-\lambda_n^2\xi\right)+\left(\frac{Br}{B^2}3^{1-n}2^{1-n}\left(1+\left(2^{n+2}3^{1-n}\right)-\eta^4B^4\right)\right) \tag{17}$$

The bulk mean temperature and Nusselt number are calculated in order to characterize the heat transfers with Eqs. (18) and (19), respectively.

$$\theta_m(\xi) = \int_0^1 u(\eta)\theta(\xi,\eta)\eta^n \mathrm{d}\eta \tag{18}$$

$$Nu = -\frac{2^{2-n}}{\theta_m}\left(\frac{\partial\theta}{\partial\eta}\right)_{\eta=1/B} \tag{19}$$

4 Results

The variations of fully developed Nusselt number values (Nu_{fd}) with respect to slip coefficient (β) at different Pe values and temperature jumps are shown in Fig. 3. We calculated the corresponding temperature jump coefficient (α) as a function of the β based on the possible linear relations from the literature data listed in Table 3. However, $\alpha = 7.13 \times \beta$ and $\alpha = 4.78 \times \beta$ cases developed very low Nusselt values which were excluded from the results. Thus, only three relations based on $\kappa = 3.03, 0.61, 0.14$ ($\alpha = \kappa \times \beta$) were studied. The Br number defining viscous heating term kept zero in Fig. 3a, b, presenting Nu_{fd} values for channel and tube flows, respectively. Nu_{fd} decreased as the velocity slip and related temperature jump increased. The decrement was much faster for $\kappa = 0.61$ and $\kappa = 3.03$ cases at β values smaller than 1.0, after which Nu_{fd} slowly converged to zero. For example, Nu_{fd} became almost zero at $\beta = 40$ for $\kappa = 0.14$, at $\beta = 10$ for $\kappa = 0.61$, and at $\beta = 2$ for $\kappa = 3.03$ the case of channel flows. These Nu_{fd} variations at low β are also given in the magnified images set in top, right corner of the plots. The case of $\kappa = 0.14$ developed negligible temperature jump ($\alpha \sim 0$) at very low β values ($\beta < 0.05$ for channel and $\beta < 0.25$ for tube) and Nu_{fd} increased at low β range. This result validates that the velocity slip enhances the convection. However, further increases in β made the temperature jump non-negligible, reduced the heat transfer from the wall, and decreased the Nu_{fd}. The effect of Pe number on fully developed Nusselts is shown in Fig. 3a, b. At low slip and jump, lower Pe flows develop higher Nu_{fd} due to axial conduction; specifically, very low temperature jumps allow axial conduction to affect convection. However, axial conduction influence on fully developed Nusselts disappears by the increase in temperature jump with the increased velocity slip. Overall, Nu_{fd} values are smaller for cylindrical geometries than rectangular geometries, although this difference becomes negligible as the temperature jump and velocity slip increases and Nu_{fd} becomes almost independent to the channel geometry. In sum, when small-scale effects become dominant, axial conduction and flow geometry dependence of heat transfer disappear.

Fully developed Nusselts of nonzero Br solution with slip and jump are given in Fig. 3c. In the presence of viscous dissipation, Nu_{fd} became independent to axial conduction and Pe number. Furthermore, Nusselt also converged to the same fully developed value independent to value of Br number. Overall, viscous heating enhanced the Nu_{fd} values which were higher than $Br = 0$ case. This increase of Nu_{fd} was mostly observed at low β cases ($\beta < 1.5$) for both cylindrical and rectangular geometries. Figure 3c also provides a comparison of channel and tube cases, while they became identical for high temperature jump values.

We would also like to underline that slip and jump coefficients are determined not only by velocity slip and temperature jump length values, but also by the characteristic flow height. For example, a constant 100 nm slip length in a 50-nm tube results in $\beta = 2$, while the 200-nm tube made from the same material decreases the β value to 0.5. This suggests that α and β coefficients calculate non-equilibrium effects as a contribution of velocity slip and temperature jump in the total mass and heat transport developing in the corresponding confinement.

Variations of local Nusselt values through thermal development length are given in Fig. 4 at different β, κ, and Pe values with zero dissipation. Specifically, Fig. 4a, b is for the rectangular and Fig. 4c, d is for the cylindrical coordinate systems. The high and low ends of the previously discussed κ values were tested at $\alpha = 0.14\beta$ as shown in Fig. 4a, c and at $\alpha = 3.03\beta$ as shown in Fig. 4b, d. Local Nusselt number showed strong variation through flow direction depending on slip and jump; the lower the β and α, the higher the variation in the thermal development region. Basically, the local Nu decreases and reaches the fully developed value at a certain length depending on Pe value of flow. The thermal development length decreases the increase of Pe as the effect of axial conduction diminishes. Pe dependence of convection was very strong in the thermal development region especially for low velocity slip and temperature jump cases. On the other hand, axial conduction effects disappeared for β values higher than 3 at low temperature jump cases ($\kappa = 0.14$) and for β values higher than 0.1 at high temperature jumps ($\kappa = 3.03$). The $Pe = 1$ results of $\beta = 0$ were also given in each figure by circular symbols for a comparison. Simply, in Fig. 4a, c, results of $\beta = 0.01$ at $\kappa = 0.14$ developed negligible small-scale effects and Nu_x values remained similar

Table 5 Coefficients of Kummer's Hypergeometric function for the solution of rectangular and circular geometries

Coefficients	$n = 0$ Cartesian system	$n = 1$ Cylindrical system
a	$\frac{1}{4} - \frac{\lambda A}{4} - \frac{16\lambda^3}{9Pe^2B^4}$	$\frac{1}{2} - \frac{\lambda A}{4} - \frac{16\lambda^3}{4Pe^2B^4}$
c	$1/2$	1
z	$x^2 = \lambda\eta^2$	$x^2 = \lambda\eta^2$

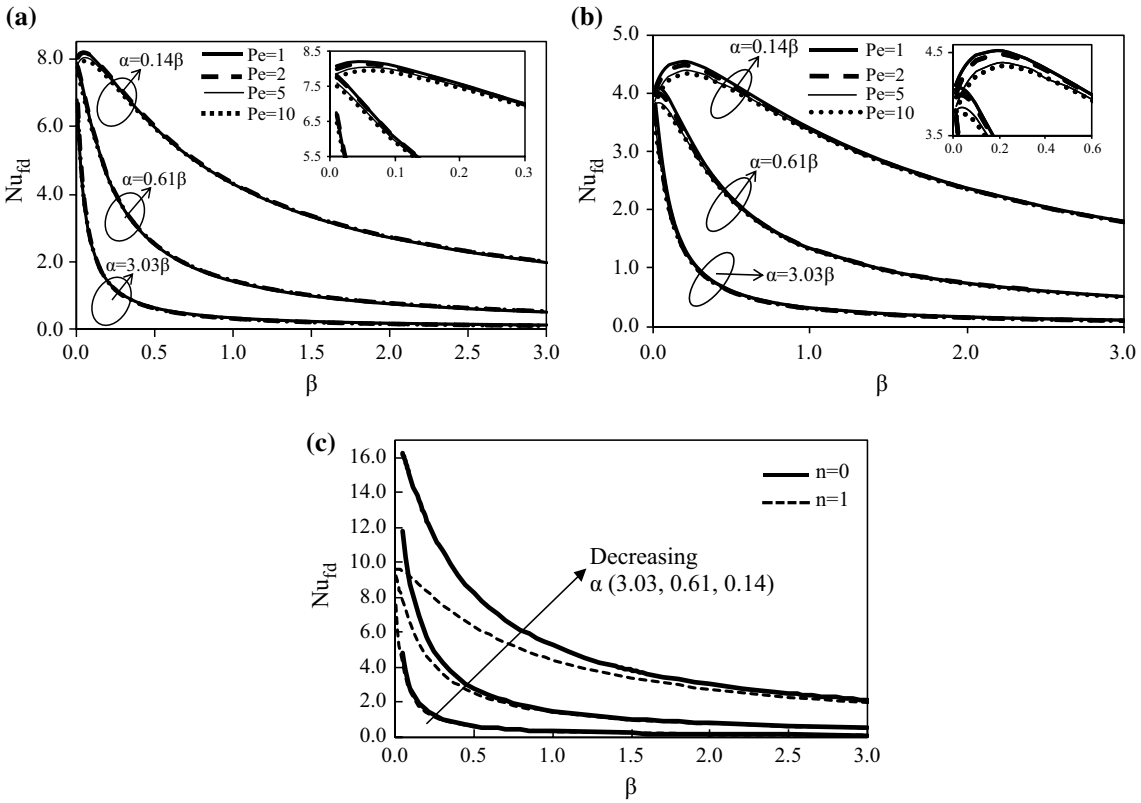

Fig. 3 Fully developed Nusselt number values as a function of β for different κ values ($\alpha = \kappa \times \beta$) **a** for $Br = 0$, $n = 0$, **b** for $Br = 0$, $n = 1$, and **c** for $Br \neq 0$

to the macroscale solution given at $\beta = 0$. However, for higher κ value of 3.03 (Fig. 4b, d), Nu_x diverged strongly from macroscale behavior even for the low β value of 0.01. In such perspective, the lowest limit of β for the development of micro-/nanoscale effects showed variation based on the model defining the L_s versus L_k relation. Hence, non-equilibrium may dominant heat transfer for β values as low as 0.01. These mechanisms were similarly observed for both geometric systems such that only the values of Nu_x and Nu_{fd} differed quantitatively.

The amount of heat transferred is not only the function of the heat transfer coefficient calculated by the Nu number, but also it is a function of temperature difference. Hence, the change in temperature through the convective flow direction should be carefully studied in addition to Nu values, but this has been mostly overlooked by the literature. For such a case, we studied the variation of dimensionless temperature (θ) in Fig. 5. Figure 5a–c presents results of slit case ($n = 0$), while Fig. 5d–f is for tube flows ($n = 1$). First, Fig. 5a, d shows the variation of θ from the center of confinements to the surface at different axial locations for a high axial conduction, negligible slip, negligible jump, and no-dissipation case ($Pe = 1$, $\alpha = 0.14\beta$, $\beta = 0.01$, and $Br = 0$). Basically, non-dimensional temperatures starting from unity at the entrance decreased to zero as it reached the wall temperature at $\xi_C \approx 2$ for slit case and $\xi_T \approx 1$ for tube. Hence, heat transfer diminishes for the rest of the flow direction as the temperature difference between wall and liquid became zero. Next, Fig. 5b, e examines the temperature profiles at $\xi_C = \xi_T = 0.5$ for different values of β in the presence of axial conduction ($Pe = 1$) and high temperature jump ($\alpha = 3.03\beta$). In order to understand the variation in temperature jump at the surface ($\eta = 1$) with the increase in β better, temperature profiles for $\beta = 0$ are also given in the figures for comparison. An increase in β increased the α, and hence, the liquid temperature value on the surface (at $\eta = 1$) became nonzero and increased. Increases in temperature jump increase the average temperature in the channel, but also decrease the amount of heat transferred from the surface as the temperature profile becomes flatter and temperature gradient almost disappears in the surface normal direction. Next, the effects of conduction toward the inlet in the axial direction are studied in Fig. 5c, f as a function of Pe for $\alpha = 0.14\beta$, while two β values were tested ($\beta = 0.01$ and $\beta = 3$). Temperature profiles measured at $\xi_C = 05$ and $\xi_T = 0.15$ were increased with the decrease in Pe, but at the same time, the temperature gradient increased as well. This enhancement was less profound for $\beta = 3$ due to high temperature jump, creating opposite effects. Overall, Fig. 5 explains that length heat transfer occurs in a limited

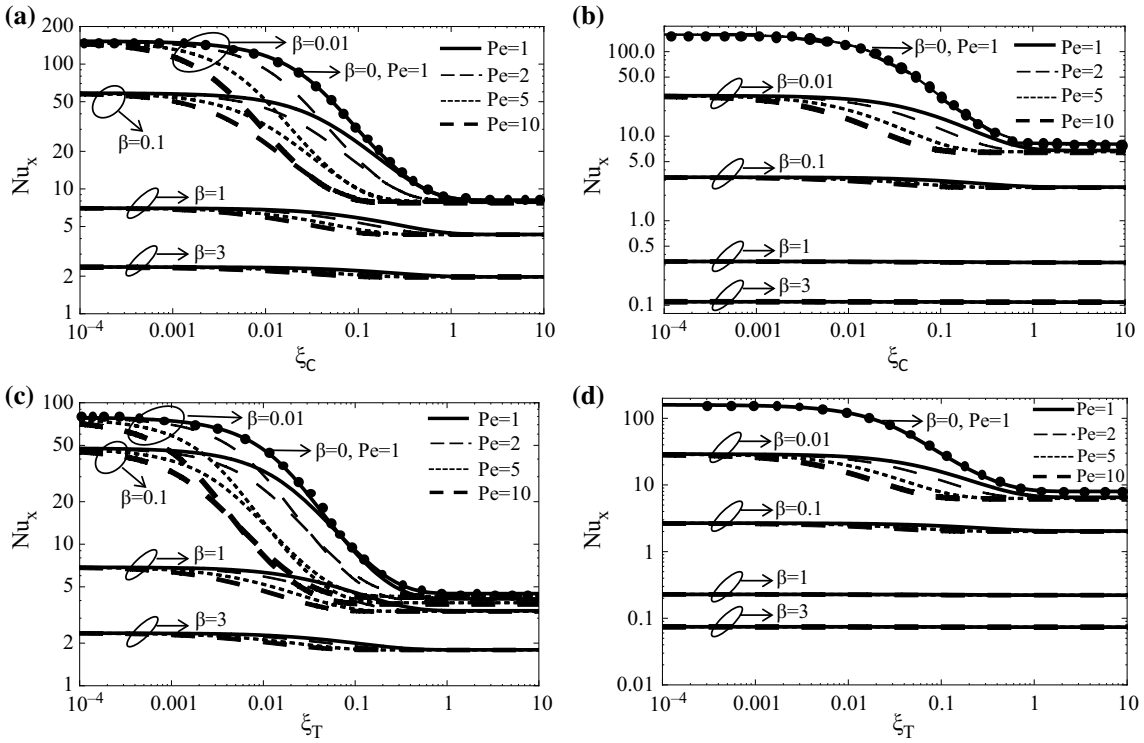

Fig. 4 Variation of local Nusselt number for $Br = 0$ cases along axial lengths of channel (ξ_C) and tube (ξ_T) for different Peclet numbers and β values at **a**, **c** $\alpha = 0.14\beta$, and **b**, **d** $\alpha = 3.03\beta$

part of the heating region for constant temperature surfaces, which is comparable to the thermal development length, after which the flow is isothermal. This behavior further demonstrates the importance of properly calculating the Nusselt number by averaging local values through thermal entrance region.

The effects of viscous dissipation on local Nusselt values at different slip coefficients at $\alpha = 0.14\beta$ and $Pe = 1$ case were investigated for positive and negative of the same Br value shown in Fig. 6a, b for slit and tube flows, respectively. For this $\kappa = 0.14$ case, small-scale effects do not develop up to $\beta = 0.1$ and the macroscale solution was similar to results at $\beta = 0.01$, and the $\beta = 0$ results were excluded for simplicity. The symbol of Br is related to heat transfer direction; Br is positive for fluid cooling and negative for fluid heating. Basically, local Nu values remained the same with no viscous dissipation case of corresponding Pe flow up to some axial location where Nu_x converged to Nu_{fd} values given in Fig. 3a, b with a sudden jump. For such a case, viscous dissipation of positive Br augmented the heat transfer and increased local Nu. However, for negative Br numbers, a singularity point formed at which the bulk mean temperature became equal to the wall temperature. After this singularity point, the direction of the heat transfer changed. The effect of viscous dissipation decreased by the increase in velocity slip and temperature jump. As β increases, Nu_{fd} decreased and the viscous dissipation effects started later as the jump point shifted to downward flow direction. The general trend in variation of local Nusselts was similar for $n = 0$ and $n = 1$ in that only the quantitative values were different.

Figure 7 further studies the effect of Br value on local Nu variation at different temperature jumps and axial conductions. For a $Pe = 1$ flow with $\beta = 0.1$, Fig. 7a, c presents Nu_x through thermal development length of slit and tube, respectively. When the temperature jump increased, viscous dissipation became almost negligible ($\alpha = 3.03\beta$). For a low temperature jump case ($\alpha = 0.14\beta$), viscous dissipation effects started earlier and covered more of the developing region with the increase in Br while the Nusselt jump point shifted toward the inlet side. Figure 7b, d studies axial conduction influence at $\beta = 0.1$ and $\alpha = 0.14\beta$ for different Br values. High Pe flows developed earlier which makes viscous dissipation effects start earlier too. At the same slip and jump, dissipation effects shifted further toward the inlet with the increase in axial conduction. The effect of the magnitude of Br was only observed in the middle of development length; dissipation had no effect on early Nu_x values, while Nu_x were independent of Pe and Br values in the late developing region and converged to identical Nu_{fd} values given in Fig. 3c for any nonzero Br flow cases.

The distributions of θ at various axial locations are investigated in Fig. 8 for positive Br values of surface heating.

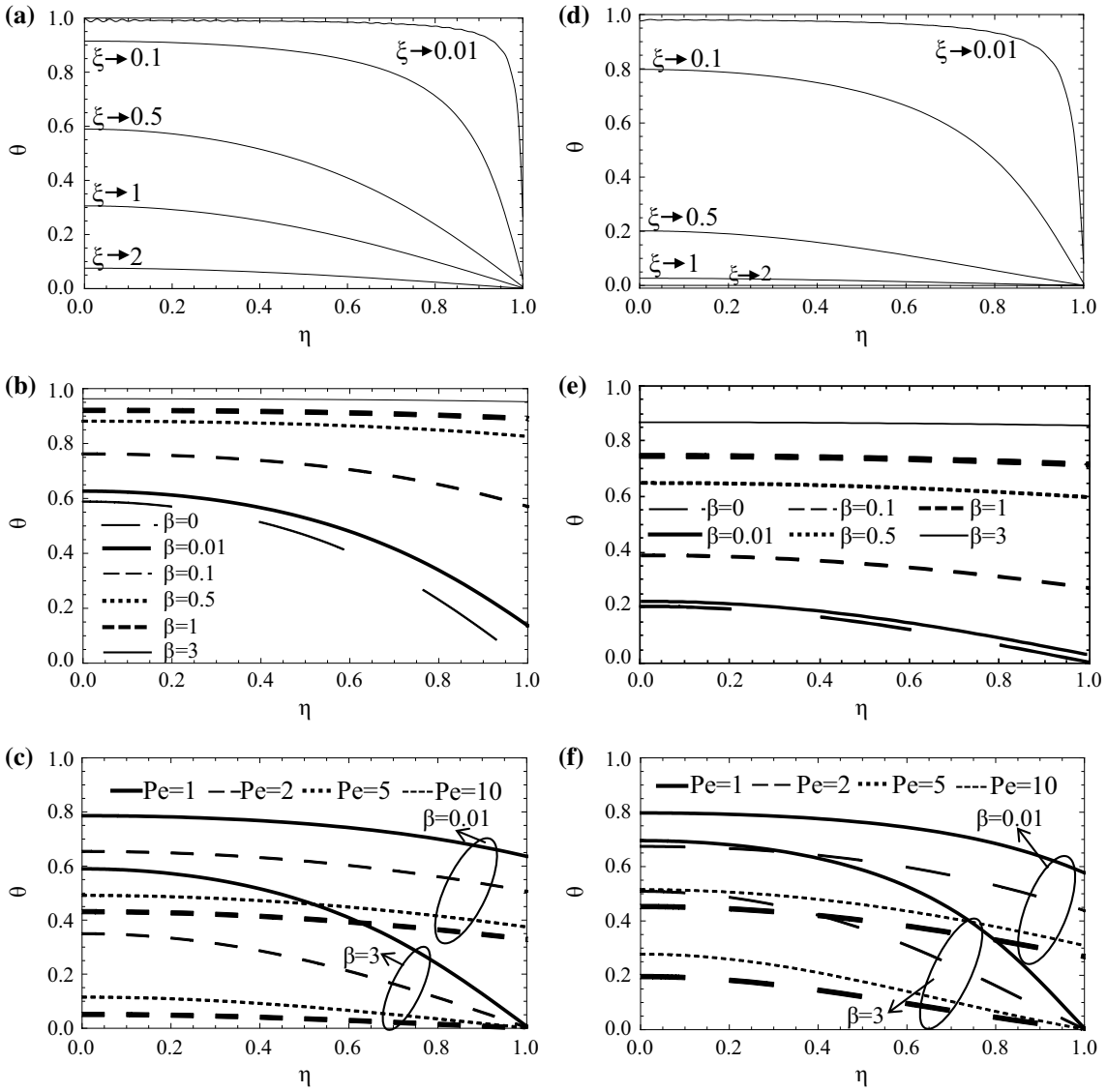

Fig. 5 Dimensionless temperature distributions in the surface normal direction for $n = 0$ (*left side*) and $n = 1$ (*right side*) at different axial locations, *Pe* numbers, β and α values

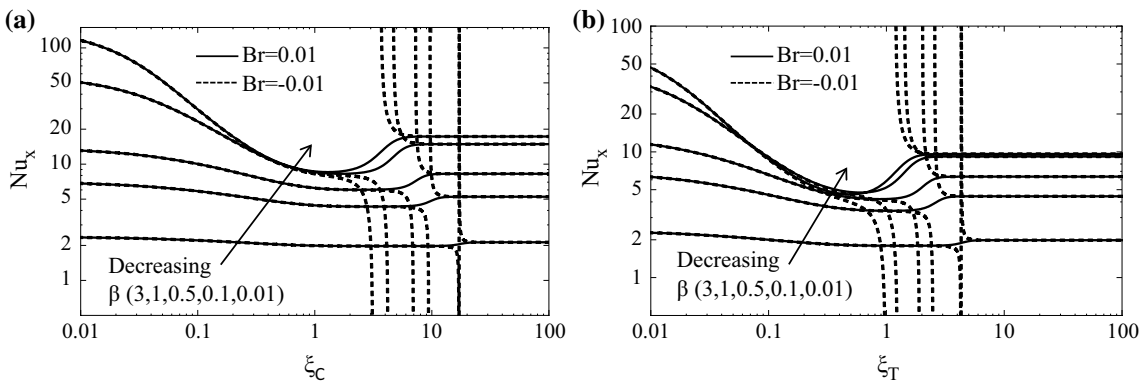

Fig. 6 Variation of local *Nu* number through **a** ξ_C and **b** ξ_T for different values of β and *Br* number at $\alpha = 0.14\beta$, and $Pe = 1$

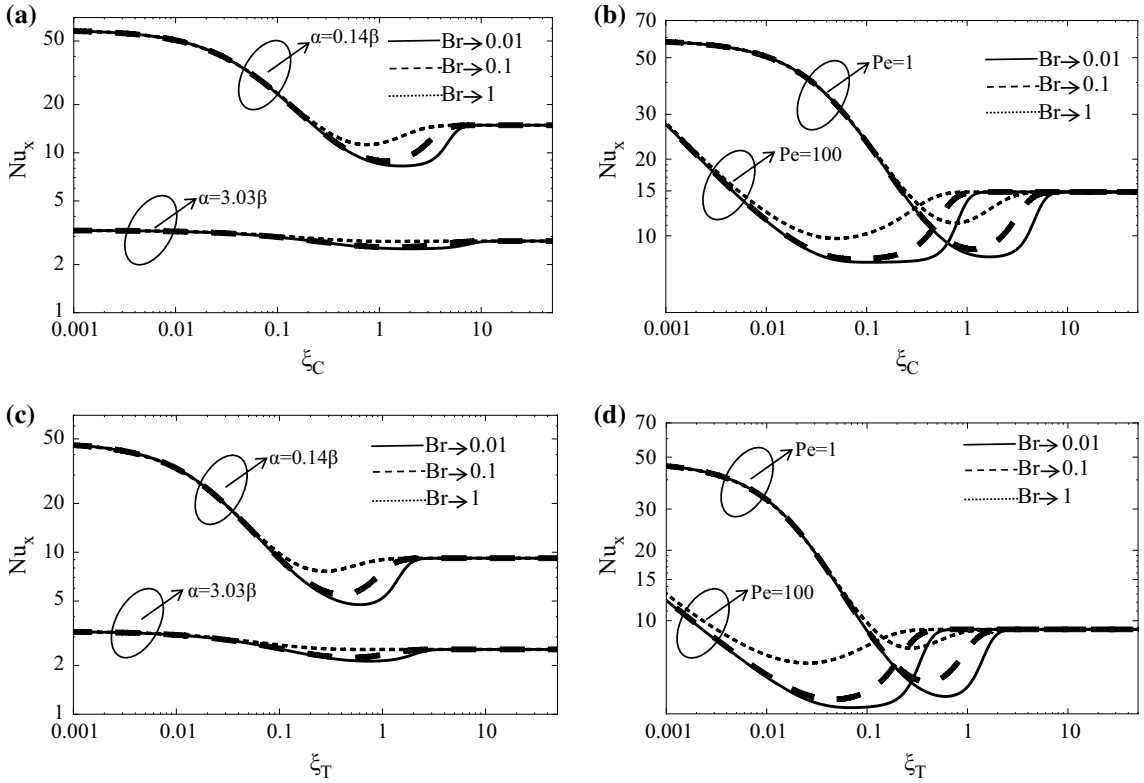

Fig. 7 Local Nusselt number variation through axial direction with different values of Brinkman number in the presence of **a**, **c** different temperature jumps and **b**, **d** different axial conductions ($n = 1$ at **a**, **b**, and $n = 0$ at **c**, **d**)

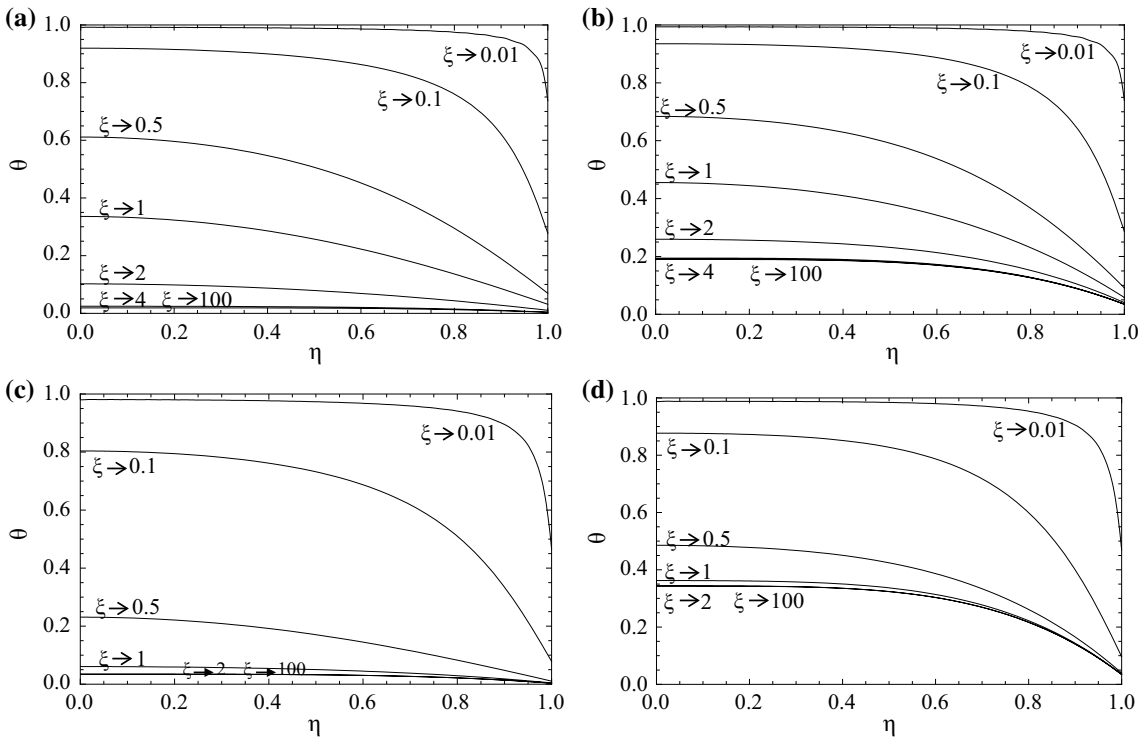

Fig. 8 Variation of dimensionless temperature in **a**, **b** slit ($n = 0$) and **c**, **d** tube ($n = 1$) geometries at different axial locations for $Pe = 1$, $\beta = 0.1$, and $\alpha = 0.14\beta$ case while $Br = 0.1$ at **a**, **c**, and $Br = 1$ at **b**, **d**

Different from no-dissipation cases, heat transfer between liquid and surface never stops. Instead, liquid losing heat has temperature decreases through the flow direction until the heat generated by viscous forces becomes equal to heat conduction at the surface. Basically, a temperature profile develops similar to no-dissipation case up to some axial location after which viscous heating develops and temperature profile remain unchanged. Such location comes earlier for tubes ($\xi_T = 2$) than slits ($\xi_C = 4$). The magnitude of viscous heating determines the developed temperature profile directly based on Br value. Higher Br values create higher liquid temperatures in the confinement and higher surface heating.

The non-dimensional temperature profiles for surface cooling (negative Br) cases are shown in Fig. 9 for $Br = -0.1$, $Pe = 1$, $\beta = 0.1$, $\alpha = 0.14\beta$. Figure 9a gives the results in a slit geometry, and temperature profiles in Fig. 9b are from tube convection. Different from the heating case, viscous heating created an adverse effect on cooling process as the dissipation increases the liquid temperature which decreases the temperature difference between liquid and hot surface, and lessens the heat transport. For such a case, a temperature profile developing similar to no-dissipation case converged to zero value faster after which heat transfer change direction and the temperature of liquid exceeded the surface temperature. Hence, viscous dissipation of liquid started heating the surface and non-dimensional temperature converged to a certain negative value depending on the equilibrium based on the Br number. Figure 9c, d shows temperature profiles during the change in heat transfer direction better using a zoomed view. Near surface liquid became warmer than the surface as well as warmer than the liquid at the center, since the viscous dissipation developed by the velocity gradient was higher near the surface. This behavior was observed stronger in the circular system since the surface related effects are more dominant due to higher surface-to-volume ratio compared to Cartesian system. Further in the axial direction, center liquid temperature heated up and the temperature profile was developed. The temperature profile became fully developed earlier for the circular geometries compared to the rectangular geometries. Hence, for the circular geometries, θ became zero at earlier points, and as a result, heat transfer ended. Also, the difference between the location where the first negativity was observed and the fully developed temperature profile reached was smaller in the circular geometries.

The effect of the viscous dissipation is shown in Fig. 10. All the parameters taken are the same as Fig. 9, except Br number ($Br = -1$). The increase in viscous dissipation made the thermal developing length smaller for rectangular geometries. On the other hand, for circular geometry, there was no visible change in terms of the axial location where θ is equal to zero. However, the singularity point moved backward to its half-length when Br folded ten times.

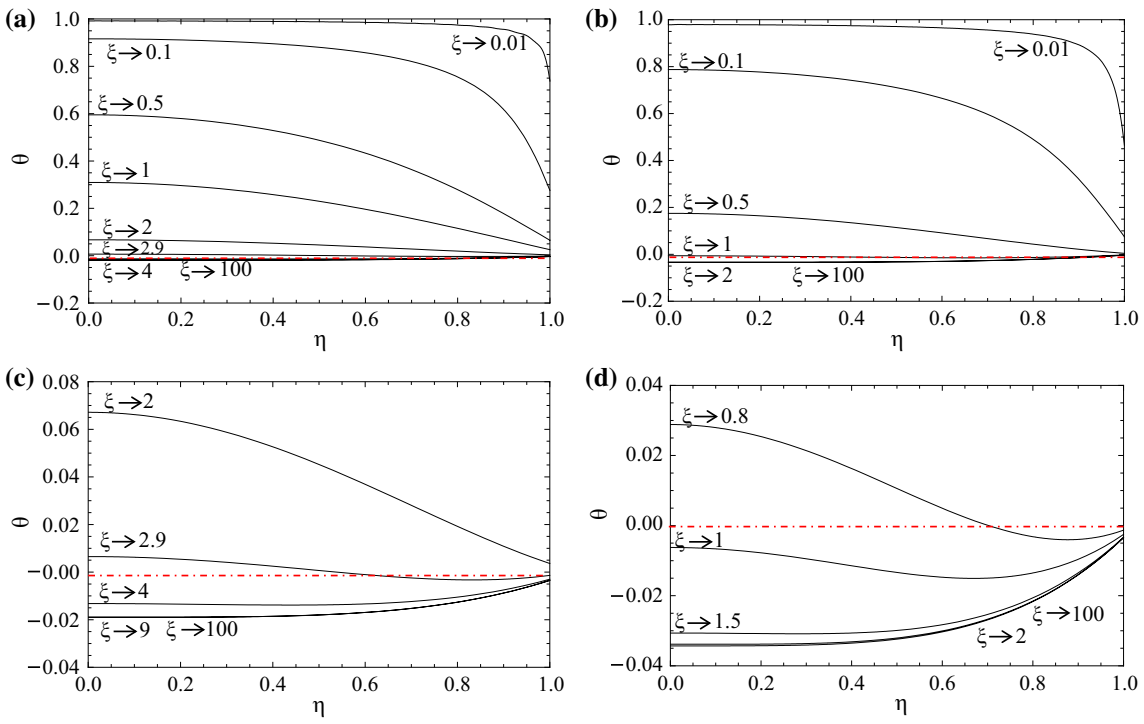

Fig. 9 Variation of dimensionless axial temperature for $n = 0$ (*left*) and $n = 1$ (*right*) through the flow direction at $Pe = 1$, $\beta = 0.1$, $\alpha = 0.14\beta$, $Br = -0.1$. **c**, **d** are the enlarged view of profiles changing sign

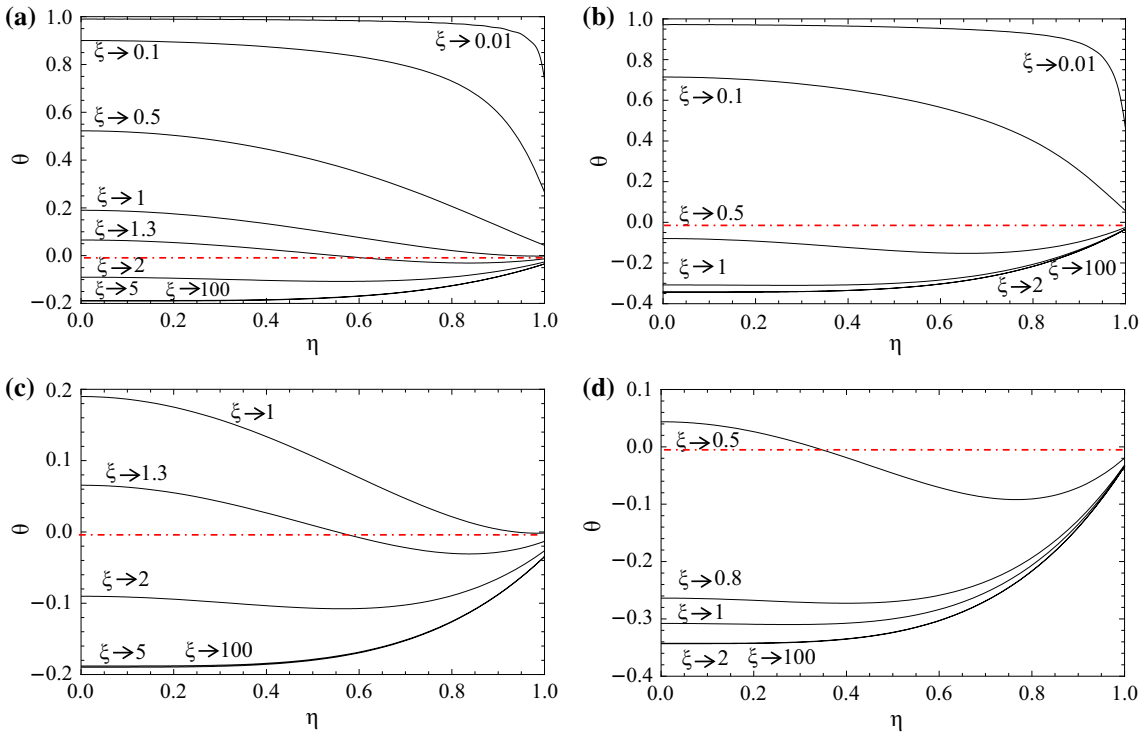

Fig. 10 Variation of dimensionless axial temperature for $n = 0$ (*left*) and $n = 1$ (*right*) through the flow direction at $Pe = 1$, $\beta = 0.1$, $\alpha = 0.14\beta$, $Br = -1$. **c**, **d** are the enlarged view of profiles changing sign

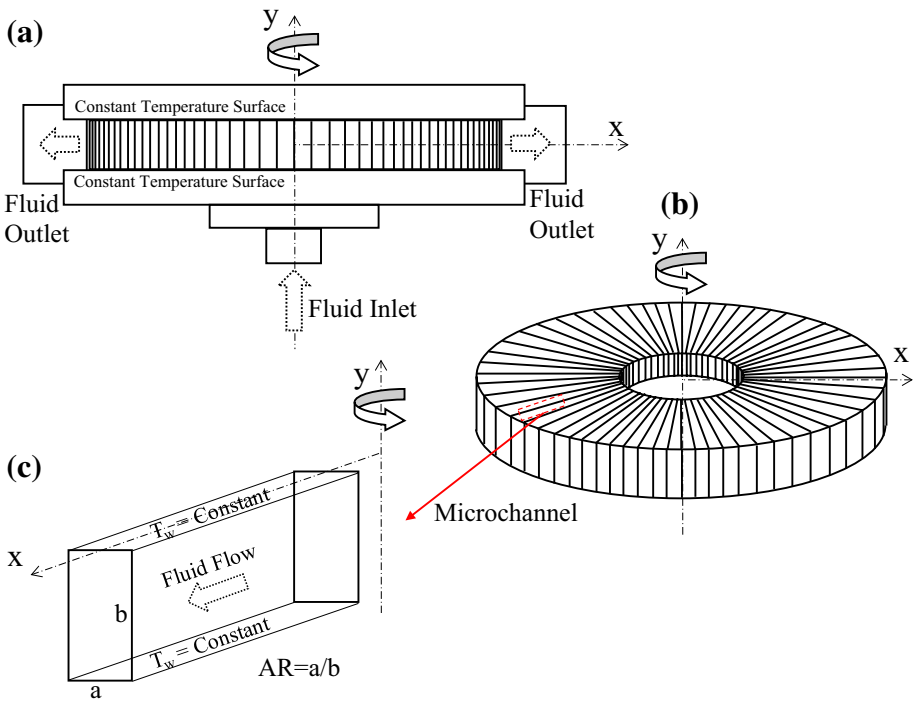

Fig. 11 Sketch of rotating micro-channels of a micro-fluidic heat exchanger along with the boundary conditions and system parameters

We further implemented our solution procedure to a micro-fluidic application in an attempt to present the differences from the calculations of existing conventional models. For such a case, we studied the conditions used in Roy et al. for the case of heat transfer in rotating rectangular micro-channels (Roy et al. 2013). Rotating micro-channels are

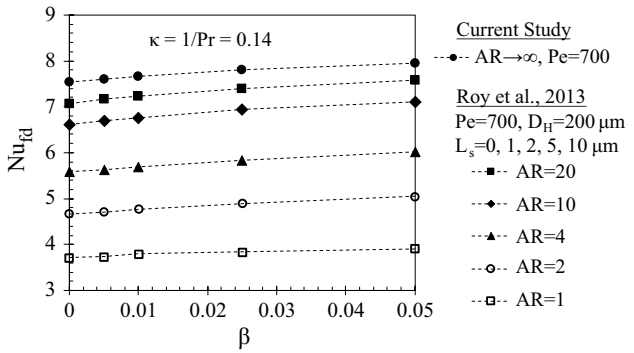

Fig. 12 Nu_{fd} values adapted from Roy et al. (2013) for the non-rotating micro-channel case in comparison with the results of current study

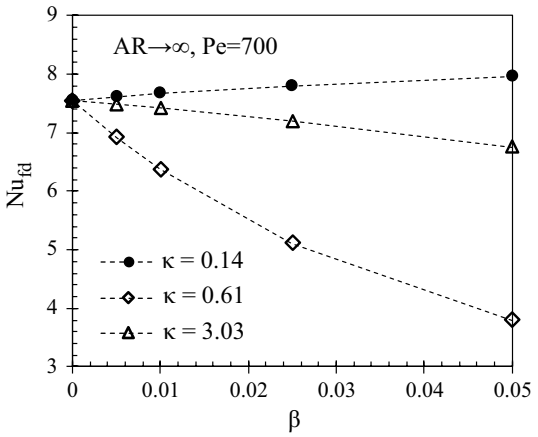

Fig. 13 Nu_{fd} calculated at the conditions of Roy et al. (2013), but at different κ values

important for biomedical and chemical separation applications. Figure 11 provides an illustration of the conceptual rotating micro-heat exchanger (Fig. 11a) described in Roy et al. Centrifugal fluid flow in micro-channels (Fig. 11b) along with the boundary conditions and system parameters (Fig. 11c) is presented.

Roy et al. studied heat transfer in such micro-channels by correlating the temperature jump boundary condition with velocity slip on the surface based on the well-known gas flow model ($L_k = L_s/Pr$) at various finite aspect ratios (AR $\leq$ 20). Since our analytical solution is based on the slit channel assumption (Height $\ll$ Depth), our results represent the case of a very high aspect ratio (AR $\rightarrow \infty$). For such a case, we compared the non-rotating channel results of Roy et al. with the results of our solution procedure at the corresponding conditions. Specifically, we calculated Nu_{fd} at Re = 100, $Pr = 7$, $\kappa = 0.14$ and $D_H = 200$ μm with different slip lengths ($L_s = 0$, 1, 2, 5, 10 μm) resulting in the slip coefficients ($\beta = L_s/D_H$) of $\beta = 0$, 0.05, 0.01, 0.025 and 0.05. Figure 12 presents Nu_{fd} from Roy et al. at different aspect ratios (AR = 1, 2, 4, 10, and 20) in comparison with our results at the same conditions, but at AR $\rightarrow \infty$. Overall, Nu_{fd} values from Roy et al. increased by the increase of β or AR. Even though we could not have a direct comparison, variation of Nu_{fd} developed in our results for AR $\rightarrow \infty$ fit well with the behavior of Nu_{fd} from the adopted data with respect to an increase in AR and β. As the AR approached to infinity, Nu_{fd} converges to well-known parallel plate solution of $Nu_{fd} = 7.54$ at $\beta = 0$ since the axial conduction is almost negligible at $Pe = 700$.

After the comparison and validation of our findings, we further studied the conditions from Roy et al. with different L_s versus L_k dependence. Figure 13 gives the Nu_{fd} of AR $\rightarrow \infty$ with different κ values calculated in Sect. 2.2 (Table 3) for the same conditions studied in Fig. 12. While an increase in Nu_{fd} was observed in Roy et al. with the increase in slip length in the studied β range, change in L_s versus L_k model developed an opposite behavior. For κ values of 0.61 and 3.03, Nu_{fd} decreased when β value increased. Results showed the dominant effect of L_s versus L_k model chosen to describe the relation between velocity slip and temperature jump of a surface.

Roy et al. did not attempt to consider any L_s versus L_k relation different from the kinetic gas theory for the case of the liquid convection. As discussed in detail through our manuscript, direct use of gas theories on liquid flows is not an adequate consideration. Even though, the L_s versus L_k relation of liquid flows can be expected to be similar to behavior observed in gas flows, the linear relationship may develop at different proportionalities at liquid cases since the momentum and heat exchange with surface are different and more complex than the gas flows. Table 3 summarizes the existing literature data on velocity slip and temperature jump values measured on the same surface for liquid flows, which simply supports this by presenting different relations (κ values) than the gas flows.

5 Conclusions

Heat transfer characteristics of liquid convection in micro-/nanoscale slits and tubes diverge from existing continuum predictions due to the non-equilibrium in liquid dynamics. But, the characterization of non-equilibrium is not simple since there is no simple theory to calculate liquid dynamics at small scales. On the other hand, liquid non-equilibrium is mostly confined near surface for flow dimensions as small as 50 nm. For such a case, an overall small-scale characterization by defining a velocity slip for the non-equilibrium at momentum transport and a temperature jump for the non-equilibrium at energy exchange through the boundaries is a simple and promising method to calculate transport in

micro-/nanoscale. However, the existing literature is misleading as the required slip and jump values are very conflicting and multiple researchers have practiced the kinetic gas theory incorrectly in the liquid cases.

Instead, this study provided the details of non-equilibrium mechanisms in liquids as well as gas domains in order to clarify their differences and explain the fallacious use of Knudsen number-based theories in liquid cases. Next, length scales of liquid non-equilibriums, such as electric double layer (EDL), density layering (DL), and interface liquid/solid coupling, were described. Molecular level analysis from the literature found EDL and DL regions mostly dominant in only 1–2 nm extent from the surfaces with the interface coupling effect right on the boundaries. Hence, we predicted the dimensional limit for a non-dimensional analytical solution of micro-/nano-liquid convection based on dynamic similarity as ~50 nm. For confinement sizes bigger than 50 nm, non-equilibrium covered a non-finite part of flow domain that above listed three near surface mechanisms can be simply modeled by the slip and jump boundary conditions. Furthermore, the literature suggested that the specific slip length of a surface/liquid couple is constant independent of size in confinements bigger than 10 nm, while similar behavior was also observed for Kapitza length. This suggests that, for a given surface and liquid, a non-dimensional form of slip or Kapitza lengths normalized with the flow dimensions can be utilized to incorporate non-equilibrium effects into well-known fluid dynamics solutions.

With a wide literature survey, we provided published slip and Kapitza length results of various liquid/solid couples. We further normalized published data with corresponding conduits sizes in an attempt to justify slip and jump coefficient ranges we targeted to study. On the other hand, the required slip and jump values could only be calculated by experiments or molecular simulations since there is no simple theory. For such a case, we discussed possible relations between velocity slip and surface wetting in order to estimate the required boundary conditions from an easy contact angle measurement. We summarized available slip length measurements accompanied with the wetting angle of corresponding surfaces and applied proposed slip versus wetting models. Based on the available data, slip length showed an exponential increase from almost negligible values to 10 nm in the 50°–150° contact angle range. We should also underline here that existing data are very limited and slip length values much higher than these were also measured in the literature (Table 1) without corresponding contact angle values. For Kapitza length values, we utilized the previously introduced direct relation between temperature jump and slip from which we developed possible linear relationships based on the literature data of jump and slip values measured on the same surface.

To include in the analytical solution of liquid convection, we determined a range of slip coefficients and calculated the jump coefficients from corresponding slip using the different linear proportionalities obtained from the fits on the literature data. Slip and jump coefficients predicted the contribution of non-equilibrium effects onto the overall momentum and energy exchange between a specific liquid and solid couple in a certain conduit size. Hence, a high value of these coefficients suggesting strong micro-/nano-effects can be developed either by a very high velocity slip length in a moderate conduit size (e.g., $L_s = 500$ nm and $H = 500$ nm) or by a moderate slip in a very small size conduit (e.g., $L_s = 50$ nm and $H = 50$ nm). These two systems are dynamically similar as long as the thickness of molecular level non-continuum mechanisms (EDL and DL) remains negligible compared to conduit size.

Small-scale effects on heat transfer were investigated in terms of fully developed Nusselt numbers first. While the velocity slip alone enhanced the convection, temperature jump developing as a function of slip created a thermal resistance which decreases the *Nu* values. Axial conduction did not create a significant effect on fully developed *Nu*, but viscous heating strongly dominated the values. For low slip and jump coefficients, *Nu* showed strong variation through the thermal development length and influence of axial conduction and viscous dissipation also became important. Hence, any heat transfer calculations should be performed by considering an average value of local Nusselt numbers through the heating length, especially for current micro-/nano-cooling applications with heating lengths comparable with confinement size. On the other hand, the high values of these coefficients made the variation through the developing region, axial conduction effect, and viscous dissipation effect negligible. Further details of energy exchange were found from developing temperature profiles. The heat transfer developed as a function of not only convection coefficient, but also the temperature difference between liquid and surface. Especially for the constant surface temperature cases, the understanding of the non-dimensional temperature variation is crucial since the heat transfer stops when the liquid temperature reaches the surface value. Results of convective heat transfer over a constant temperature surface will provide insight for the current thermal management attempts using phase changing materials creating constant surface temperatures in contact with heat exchanger liquids.

Acknowledgements Authors would like to thank Izmir Institute of Technology for the support under the Grant Number 2016-IYTE-36. Murat Barisik would like to thank The Scientific and Technological Research Council of Turkey (TUBITAK), cofunded by Marie Curie Actions under FP7 for support under the Grant Number TUBITAK 115C026.

References

Akbarinia A, Abdolzadeh M, Laur R (2011) Critical investigation of heat transfer enhancement using nanofluids in microchannels with slip and non-slip flow regimes. Appl Therm Eng 31(4):556–565

Arfken GB, Weber HJ (2005) Mathematical methods for physicists' international student edition. Academic press, New York

Atalay S et al (2014) Surface charge of a nanoparticle interacting with a flat substrate. J Phys Chem C 118(20):10927–10935

Bardia R et al (2016) Continuum and molecular-dynamics simulation of nanodroplet collisions. Phys Rev E 93(5):053104

Barisik M, Beskok A (2011a) Molecular dynamics simulations of shear-driven gas flows in nano-channels. Microfluid Nanofluid 11(5):611–622

Barisik M, Beskok A (2011b) Equilibrium molecular dynamics studies on nanoscale-confined fluids. Microfluid Nanofluid 11(3):269–282

Barisik M, Beskok A (2012a) Surface–gas interaction effects on nanoscale gas flows. Microfluid Nanofluid 13(5):789–798

Barisik M, Beskok A (2012b) Boundary treatment effects on molecular dynamics simulations of interface thermal resistance. J Comput Phys 231(23):7881–7892

Barisik M, Beskok A (2013) Wetting characterisation of silicon (1, 0, 0) surface. Mol Simul 39(9):700–709

Barisik M, Beskok A (2014a) Scale effects in gas nano flows. Phys Fluids 26(5):052003

Barisik M, Beskok A (2014b) Temperature dependence of thermal resistance at the water/silicon interface. Int J Therm Sci 77:47–54

Barisik M, Beskok A (2015) Molecular free paths in nanoscale gas flows. Microfluid Nanofluid 18(5-6):1365–1371

Barisik M, Beskok A (2016) "Law of the nano-wall" in nano-channel gas flows. Microfluid Nanofluid 20(3):1–9

Barisik M, Kim B, Beskok A (2010) Smart wall model for molecular dynamics simulations of nanoscale gas flows. Commun Comput Phys 7(5):977

Barisik M et al (2014) Size dependent surface charge properties of silica nanoparticles. J Phys Chem C 118(4):1836–1842

Barisik M et al (2015) Analytical solution of thermally developing microtube heat transfer including axial conduction, viscous dissipation, and rarefaction effects. Int Commun Heat Mass Transf 67:81–88

Barrat J-L, Bocquet L (1999) Large slip effect at a nonwetting fluid–solid interface. Phys Rev Lett 82(23):4671

Buongiorno J (2006) Convective transport in nanofluids. J Heat Transf 128(3):240–250

Byun D et al (2008) Direct measurement of slip flows in superhydrophobic microchannels with transverse grooves. Phys Fluids 20(11):113601 **(1994-present)**

Cao B-Y, Chen M, Guo Z-Y (2006) Liquid flow in surface-nanostructured channels studied by molecular dynamics simulation. Phys Rev E 74(6):066311

Cheng J-T, Giordano N (2002) Fluid flow through nanometer-scale channels. Phys Rev E 65(3):031206

Cheng YP, Teo CJ, Khoo BC (2009) Microchannel flows with superhydrophobic surfaces: effects of Reynolds number and pattern width to channel height ratio. Phys Fluids 21(12):122004

Cho J-HJ, Law BM, Rieutord F (2004) Dipole-dependent slip of Newtonian liquids at smooth solid hydrophobic surfaces. Phys Rev Lett 92(16):166102

Choi C-H, Kim C-J (2006) Large slip of aqueous liquid flow over a nanoengineered superhydrophobic surface. Phys Rev Lett 96(6):066001

Choi C-H, Johan K, Westin A, Breuer KS (2003) Apparent slip flows in hydrophilic and hydrophobic microchannels. Phys Fluids 15(10):2897–2902 **(1994-present)**

Chun M-S, Lee S (2005) Flow imaging of dilute colloidal suspension in PDMS-based microfluidic chip using fluorescence microscopy. Colloids Surf A 267(1):86–94

Cole KD, Cetin B (2011) The effect of axial conduction on heat transfer in a liquid microchannel flow. Int J Heat Mass Transf 54(11):2542–2549

Cottin-Bizonne C et al (2002) Nanorheology: an investigation of the boundary condition at hydrophobic and hydrophilic interfaces. Eur Phys J E 9(1):47–53

Cottin-Bizonne C et al (2005) Boundary slip on smooth hydrophobic surfaces: intrinsic effects and possible artifacts. Phys Rev Lett 94(5):056102

Cowley A, Maynes D, Crockett J (2014) Effective temperature jump length and influence of axial conduction for thermal transport in superhydrophobic channels. Int J Heat Mass Transf 79:573–583

Cowley A, Maynes D, Crockett J (2016) Inertial effects on thermal transport in superhydrophobic microchannels. Int J Heat Mass Transf 101:121–132

Craig VSJ, Neto C, Williams DRM (2001) Shear-dependent boundary slip in an aqueous Newtonian liquid. Phys Rev Lett 87(5):054504

Davis AMJ, Lauga E (2009) Geometric transition in friction for flow over a bubble mattress. Phys Fluids 21(1):011701

Dutta P, Beskok A (2001) Analytical solution of combined electroosmotic/pressure driven flows in two-dimensional straight channels: finite Debye layer effects. Anal Chem 73(9):1979–1986

Dutta P, Horiuchi K, Yin HM (2006) Thermal characteristics of mixed electroosmotic and pressure-driven microflows. Comput Math Appl 52(5):651–670

Enright R et al (2010) Analysis and simulation of heat transfer in a superhydrophobic microchannel. In: 2010 14th International heat transfer conference. American Society of Mechanical Engineers

Falk K et al (2010) Molecular origin of fast water transport in carbon nanotube membranes: superlubricity versus curvature dependent friction. Nano Lett 10(10):4067–4073

Gad-el-Hak M (1999) The fluid mechanics of microdevices—the Freeman scholar lecture. J Fluids Eng 121(1):5–33

Ge Z, Cahill DG, Braun PV (2006) Thermal conductance of hydrophilic and hydrophobic interfaces. Phys Rev Lett 96(18):186101

Ghorbanian J, Beskok A (2016) Scale effects in nano-channel liquid flows. Microfluid Nanofluid 20(8):121

Groombridge M, Schneemilch M, Quirke N (2011) Slip boundaries in nanopores. Mol Simul 37(12):1023–1030

Holt JK et al (2006) Fast mass transport through sub-2-nanometer carbon nanotubes. Science 312(5776):1034–1037

Hooman K, Ejlali A (2010) Effects of viscous heating, fluid property variation, velocity slip, and temperature jump on convection through parallel plate and circular microchannels. Int Commun Heat Mass Transf 37(1):34–38

Hooman K, Hooman F, Famouri M (2009) Scaling effects for flow in micro-channels: variable property, viscous heating, velocity slip, and temperature jump. Int Commun Heat Mass Transf 36(2):192–196

Huang P, Breuer KS (2007) Direct measurement of slip length in electrolyte solutions. Phys Fluids 19(2):028104 **(1994-present)**

Huang DM et al (2008) Water slippage versus contact angle: a quasiuniversal relationship. Phys Rev Lett 101(22):226101

Iverson BD, Cremaschi L, Garimella SV (2009) Effects of discrete-electrode configuration on traveling-wave electrohydrodynamic pumping. Microfluid Nanofluid 6(2):221–230

Jabbarzadeh A, Atkinson JD, Tanner RI (1999) Wall slip in the molecular dynamics simulation of thin films of hexadecane. J Chem Phys 110(5):2612–2620

Joseph P, Tabeling P (2005) Direct measurement of the apparent slip length. Phys Rev E 71(3):035303

Joseph P et al (2006) Slippage of water past superhydrophobic carbon nanotube forests in microchannels. Phys Rev Lett 97(15):156104

Kalyoncu G, Barisik M (2016) The extended Graetz problem for microslit geometries; analytical coupling of rarefaction, axial conduction and viscous dissipation. Int J Therm Sci 110:261–269
Kassinos SC et al (2004) Flow of aqueous solutions in carbon nanotubes. Berlin Heidelberg, Multiscale Modelling and Simulation. Springer, pp 215–226
Khare R, Keblinski P, Yethiraj A (2006) Molecular dynamics simulations of heat and momentum transfer at a solid–fluid interface: relationship between thermal and velocity slip. Int J Heat Mass Transf 49(19):3401–3407
Kim BH, Beskok A, Cagin T (2008) Molecular dynamics simulations of thermal resistance at the liquid-solid interface. J Chem Phys 129(17):174701
Kim BH, Beskok A, Cagin T (2010) Viscous heating in nanoscale shear driven liquid flows. Microfluid Nanofluid 9(1):31–40
Koev ST et al (2010) Chitosan: an integrative biomaterial for lab-on-a-chip devices. Lab Chip 10(22):3026–3042
Koo J, Kleinstreuer C (2003) Liquid flow in microchannels: experimental observations and computational analyses of microfluidics effects. J Micromech Microeng 13(5):568
Kou ZH, Bai ML (2011) Effects of wall slip and temperature jump on heat and mass transfer characteristics of an evaporating thin film. Int Commun Heat Mass Transf 38(7):874–878
Kuo C-C, Hsu H-J (2013) Development and application of hybrid mold with microfeatures in micro-hot embossing. Mater Manuf Process 28(11):1203–1208
Koumoutsakos P, Jaffe RI, Werder T, Walther JH (2003) On the validity of the no-slip condition in nanofluidics. In: Nano fluidics and transport. Technical proceedings of the 2003 nanotechnology conference and trade show, Nanotech, vol 1, Nano science and technology institute, pp 148–151
Lauga E, Brenner M, Stone H (2007) Microfluidics: the no-slip boundary condition. Springer handbook of experimental fluid mechanics. Springer, Berlin, pp 1219–1240
Lee C, Kim CJ (2009) Maximizing the giant liquid slip on superhydrophobic microstructures by nanostructuring their sidewalls. Langmuir 25(21):12812–12818
Lee KP, Leese H, Mattia D (2012) Water flow enhancement in hydrophilic nanochannels. Nanoscale 4(8):2621–2627
Li L, Mo J, Li Z (2014) Flow and slip transition in nanochannels. Phys Rev E 90(3):033003
Lichter S et al (2007) Liquid slip in nanoscale channels as a rate process. Phys Rev Lett 98(22):226001
Maali A, Bhushan B (2012) Measurement of slip length on superhydrophobic surfaces. Philos Trans R Soc Lond A Math Phys Eng Sci 370(1967):2304–2320
Majumder M et al (2005) Nanoscale hydrodynamics: enhanced flow in carbon nanotubes. Nature 438(7064):44
Majumder M, Chopra N, Hinds BJ (2011) Mass transport through carbon nanotube membranes in three different regimes: ionic diffusion and gas and liquid flow. ACS Nano 5(5):3867–3877
Manca O et al (2011) Numerical study of a confined slot impinging jet with nanofluids. Nanoscale Res Lett 6(1):1–16
Martini A et al (2008) Slip at high shear rates. Phys Rev Lett 100(20):206001
Matin MR, Mirdamadi HR, Ghayour M (2013) Effects of nonlocal elasticity and slip condition on vibration of nano-plate coupled with fluid flow. Physica E 48:85–95
Maynes D et al (2013) Analysis of laminar slip-flow thermal transport in microchannels with transverse rib and cavity structured superhydrophobic walls at constant heat flux. J Heat Transf 135(2):021701
Milo R, Phillips R (2015) Cell biology by the numbers. Garland Sci, New York
Mirramezani M, Mirdamadi HR (2012) The effects of Knudsen-dependent flow velocity on vibrations of a nano-pipe conveying fluid. Arch Appl Mech 82(7):879–890
Morini GL, Spiga M (2007) The role of the viscous dissipation in heated microchannels. J Heat Transf 129(3):308–318
NASA (2017) Phase change heat exchanger project (Phase Change HX)—04.05.17. NASA website. https://www.nasa.gov/mission_pages/station/research/experiments/2077.html. Accessed 07 June 2017
Navier CLMH (1823) Mémoire sur les lois du Mouvement des Fluides. Mémoires de l'Académie Royale des Sciences de l'Institut de France (Mém. Acad. R. Sci. Inst. Fr.), vol 6, pp 389–440
Neto C et al (2005) Boundary slip in Newtonian liquids: a review of experimental studies. Rep Prog Phys 68(12):2859
Ng C-O, Wang CY (2010) Apparent slip arising from Stokes shear flow over a bidimensional patterned surface. Microfluid Nanofluid 8(3):361–371
Ou J, Perot B, Rothstein JP (2004) Laminar drag reduction in microchannels using ultrahydrophobic surfaces. Phys Fluids 16(12):4635–4643 **(1994-present)**
Pham A, Barisik M, Kim B (2013) Pressure dependence of Kapitza resistance at gold/water and silicon/water interfaces. J Chem Phys 139(24):244702
Pham AT, Barisik M, Kim B (2014) Molecular dynamics simulations of Kapitza length for argon–silicon and water–silicon interfaces. Int J Precis Eng Manuf 15(2):323–329
Pham AT, Barisik M, Kim BH (2016) Interfacial thermal resistance between the graphene-coated copper and liquid water. Int J Heat Mass Transf 97:422–431
Qin X et al (2011) Measurement of the rate of water translocation through carbon nanotubes. Nano Lett 11(5):2173–2177
Qiu T et al. (2014) Swimming by reciprocal motion at low Reynolds number. Nat Commun 5:5119
Ramos-Alvarado B, Kumar S, Peterson GP (2016) Hydrodynamic slip in silicon nanochannels. Phys Rev E 93(3):033117
Rashidi V, Mirdamadi HR, Shirani E (2012) A novel model for vibrations of nanotubes conveying nanoflow. Comput Mater Sci 51(1):347–352
Rogers BJ, Wirth MJ (2012) Slip flow through colloidal crystals of varying particle diameter. ACS Nano 7(1):725–731
Roy P, Anand NK, Banerjee D (2013) Liquid slip and heat transfer in rotating rectangular microchannels. Int J Heat Mass Transf 62:184–199
Schmatko T, Hervet H, Leger L (2005) Friction and slip at simple fluid-solid interfaces: the roles of the molecular shape and the solid–liquid interaction. Phys Rev Lett 94(24):244501
Sendner C et al (2009) Interfacial water at hydrophobic and hydrophilic surfaces: slip, viscosity, and diffusion. Langmuir 25(18):10768–10781
Shi Z, Barisik M, Beskok A (2012) Molecular dynamics modeling of thermal resistance at argon–graphite and argon–silver interfaces. Int J Therm Sci 59:29–37
Shojaeian M, Koşar A (2014) Convective heat transfer and entropy generation analysis on Newtonian and non-Newtonian fluid flows between parallel-plates under slip boundary conditions. Int J Heat Mass Transf 70:664–673
Sofos F, Karakasidis TE, Liakopoulos A (2013) Parameters affecting slip length at the nanoscale. J Comput Theor Nanosci 10(3):648–650
Sokhan VP, Nicholson D, Quirke N (2001) Fluid flow in nanopores: an examination of hydrodynamic boundary conditions. J Chem Phys 115(8):3878–3887
Su Y et al (2014) Photochemical transformations accelerated in continuous-flow reactors: basic concepts and applications. Chem A Eur J 20(34):10562–10589

Suk ME, Aluru NR (2013) Molecular and continuum hydrodynamics in graphene nanopores. RSC Adv 3(24):9365–9372

Sun J et al (2012) Multi-scale study of liquid flow in micro/nanochannels: effects of surface wettability and topology. Microfluid Nanofluid 12(6):991–1008

Sun J, Wang W, Wang HS (2013a) Dependence between velocity slip and temperature jump in shear flows. J Chem Phys 138(23):234703

Sun J, Wang W, Wang HS (2013b) Dependence of nanoconfined liquid behavior on boundary and bulk factors. Phys Rev E 87(2):023020

Teo CJ, Khoo BC (2010) Flow past superhydrophobic surfaces containing longitudinal grooves: effects of interface curvature. Microfluid Nanofluid 9(2-3):499–511

Thekkethala JF, Sathian SP (2015) The effect of graphene layers on interfacial thermal resistance in composite nanochannels with flow. Microfluid Nanofluid 18(4):637–648

Thomas JA, McGaughey AJ (2008) Reassessing fast water transport through carbon nanotubes. Nano Lett 8(9):2788–2793

Thomas JA, McGaughey AJH, Kuter-Arnebeck O (2010) Pressure-driven water flow through carbon nanotubes: insights from molecular dynamics simulation. Int J Therm Sci 49(2):281–289

Tretheway DC, Meinhart CD (2002) Apparent fluid slip at hydrophobic microchannel walls. Phys Fluids 14(3):L9–L12 **(1994-present)**

Viskanta R (1983) Phase change heat transfer. Sol Heat Storage: Latent Heat Mater 1:153–222

Viskanta R (1985) Natural convection in melting and solidification. In: Kakac S et al. (eds) Natural convection: fundamentals and applications, Hemisphere, Washington, DC, pp 845–877

Vo TQ, Kim B (2015) Interface thermal resistance between liquid water and various metallic surfaces. Int J Precis Eng Manuf 16(7):1341–1346

Voronov RS, Papavassiliou DV, Lee LL (2006) Boundary slip and wetting properties of interfaces: correlation of the contact angle with the slip length. J Chem Phys 124(20):204701

Voronov RS, Papavassiliou DV, Lee LL (2007) Slip length and contact angle over hydrophobic surfaces. Chem Phys Lett 441(4):273–276

Whitby M et al (2008) Enhanced fluid flow through nanoscale carbon pipes. Nano Lett 8(9):2632–2637

Woolford B, Maynes D, Webb BW (2009) Liquid flow through microchannels with grooved walls under wetting and superhydrophobic conditions. Microfluid Nanofluid 7(1):121–135

Xu J, Li Y (2007) Boundary conditions at the solid–liquid surface over the multiscale channel size from nanometer to micron. Int J Heat Mass Transf 50(13):2571–2581

Yang X, Zheng ZC (2010) Effects of channel scale on slip length of flow in micro/nanochannels. J Fluids Eng 132(6):061201

Yang C et al (2015) Effect of temperature jump on forced convective transport of nanofluids in the continuum flow and slip flow regimes. Chem Eng Sci 137:730–739

Yasuoka H et al (2015) Confinement effects on liquid-flow characteristics in carbon nanotubes. Phys Rev E 92(6):063001

Yeh K-Y, Cho K-H, Chen L-J (2009) Preparation of superhydrophobic surfaces of hierarchical structure of hybrid from nanoparticles and regular pillar-like pattern†† Part of the" Langmuir 25th year: wetting and superhydrophobicity" special issue. Langmuir 25(24):14187–14194

Yen T-H (2015) Effects of wettability and interfacial nanobubbles on flow through structured nanochannels: an investigation of molecular dynamics. Mol Phys 113(23):3783–3795

Yen T-H, Soong C-Y (2016) Effective boundary slip and wetting characteristics of water on substrates with effects of surface morphology. Mol Phys 114(6):797–809

Yoshida J, Kim H, Nagaki A (2011) Green and sustainable chemical synthesis using flow microreactors. Chemsuschem 4(3):331–340

Zalba B et al (2003) Review on thermal energy storage with phase change: materials, heat transfer analysis and applications. Appl Therm Eng 23(3):251–283

Zhang C, Chen Y (2014) Slip behavior of liquid flow in rough nanochannels. Chem Eng Process 85:203–208